AD-A112 785 OHIO STATE UNIV COLUMBUS ELECTROSCIENCE LAB F/G 9/5
NEAR FIELD SOLUTIONS FOR ANTENNAS ON ELLIPTIC CYLINDER.(U)
JUL 77 N WANG N00019-77-C-0299
UNCLASSIFIED ESL-784685-1 NL

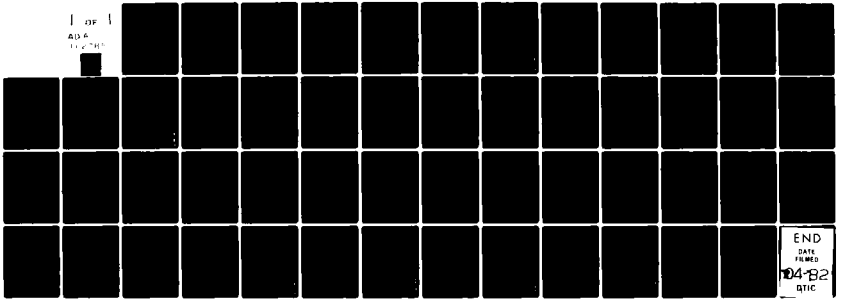

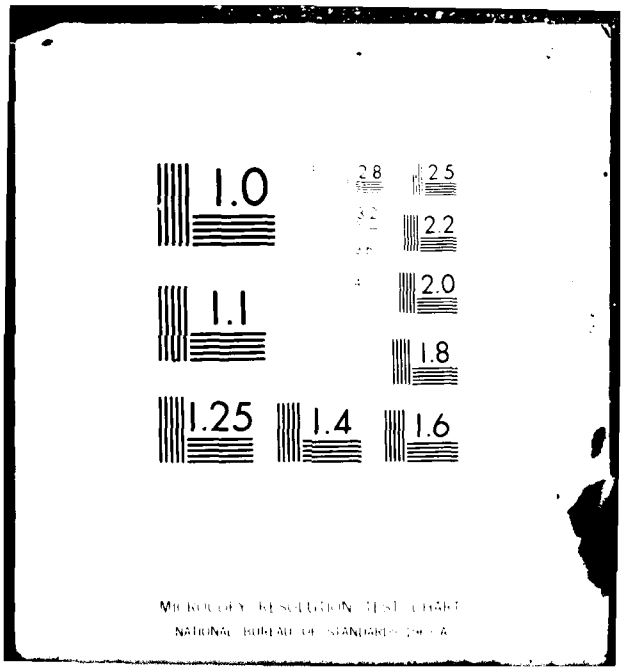
1.0
1.1
1.25
1.4
1.6
2.8
2.5
2.2
2.0
1.8

NEAR FIELD SOLUTIONS FOR ANTENNAS ON ELLIPTIC CYLINDER

Nan Wang

The Ohio State University

ElectroScience Laboratory

Department of Electrical Engineering
Columbus, Ohio 43212

Quarterly Report 784685-1

July 1977

Contract No. N00019-77-C-0299

Department of the Navy
Naval Air Systems Command
Washington, D.C. 20361

NOTICES

When Government drawings, specifications, or other data are used for any purpose other than in connection with a definitely related Government procurement operation, the United States Government thereby incurs no responsibility nor any obligation whatsoever, and the fact that the Government may have formulated, furnished, or in any way supplied the said drawings, specifications, or other data, is not to be regarded by implication or otherwise as in any manner licensing the holder or any other person or corporation, or conveying any rights or permission to manufacture, use, or sell any patented invention that may in any way be related thereto.

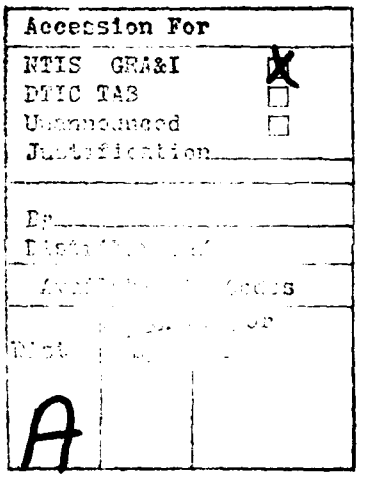

UNCLASSIFIED
SECURITY CLASSIFICATION OF THIS PAGE (When Data Entered)

REPORT DOCUMENTATION PAGE	READ INSTRUCTIONS BEFORE COMPLETING FORM
1 REPORT NUMBER	2 GOVT ACCESSION NO. AD-A112 785 / 3 RECIPIENT'S CATALOG NUMBER
4 TITLE (and Subtitle) NEAR FIELD SOLUTIONS FOR ANTENNAS ON ELLIPTIC CYLINDER	5 TYPE OF REPORT & PERIOD COVERED Quarterly Report March 15 to June 14, 1977
	6 PERFORMING ORG. REPORT NUMBER ESL 784685-1
7 AUTHOR(s) Nan Wang	8 CONTRACT OR GRANT NUMBER(s) N00019-77-C-0299
9 PERFORMING ORGANIZATION NAME AND ADDRESS The Ohio State University ElectroScience Laboratory, Department of Electrical Engineering, Columbus, Ohio 43212	10 PROGRAM ELEMENT, PROJECT, TASK AREA & WORK UNIT NUMBERS Project N00019-77-PR-RJ001
11 CONTROLLING OFFICE NAME AND ADDRESS Department of the Navy Naval Air Systems Command Washington, D.C. 20361	12 REPORT DATE July 1977
	13 NUMBER OF PAGES 48
14 MONITORING AGENCY NAME & ADDRESS(if different from Controlling Office)	15 SECURITY CLASS. (of this report) Unclassified
	15a DECLASSIFICATION/DOWNGRADING SCHEDULE N/A

16 DISTRIBUTION STATEMENT (of this Report)

APPROVED FOR PUBLIC RELEASE: DISTRIBUTION UNLIMITED

17 DISTRIBUTION STATEMENT (of the abstract entered in Block 20, if different from Report)

18 SUPPLEMENTARY NOTES

19 KEY WORDS (Continue on reverse side if necessary and identify by block number)

Slot antenna
General elliptic cylinder
High frequency solution
Near zone field
Fock functions
Local phenomena

20 ABSTRACT (Continue on reverse side if necessary and identify by block number)

Near-zone radiation characteristics for antennas on elliptic cylinders are investigated. Integral representations in terms of Fock functions for the radiated fields are employed throughout the entire space surrounding the cylinder. In the illuminated region, uniform representations employing Fock functions are used. This integral representation recovers the geometric-optics solution when the field point is far away from the lit-dark boundaries. In the shadow region, an asymptotic solution in terms

DD FORM 1 JAN 73 1473 EDITION OF 1 NOV 65 IS OBSOLETE

UNCLASSIFIED
SECURITY CLASSIFICATION OF THIS PAGE (When Data Entered)

20.

of Fock functions is obtained from the canonical problem of antennas radiating from a circular cylinder. This integral representation reduces to the creeping-wave (residue) series representation in the deep shadow region. Smooth, continuous patterns are observed for fields across the lit-dark boundaries. The solutions obtained for a circular cylinder are then generalized to elliptic cylinders on the basis of the local nature of high-requency propagation.

This report presents the theory and numerical results for the near-zone fields due to antennas mounted on circular and elliptic cylinders. Excellent agreement is obtained between the high-frequency asymptotic solutions and other solutions to the same problem.

CONTENTS

I. INTRODUCTION

If modern airborne radiating systems are to function properly, the antenna pattern must meet certain specifications. In fact, system performance is often very much dependent upon the resulting patterns. The usual design procedure for an airborne antenna consists of allocating specific locations for the antenna based primarily upon convenience with regard to aircraft structure specifications. Measurements are then used to evaluate the performance of the antenna system in terms of its desired pattern. This approach of airborne antenna design requires a great deal of engineering time and money. Thus, the need for an analytical approach which provides the antenna pattern performance in the presence of an airframe is quite apparent.

One of the approaches that has found great success for analyzing on-aircraft antennas is the Geometrical Theory of Diffraction (GTD). The GTD is a high frequency asymptotic solution in which the scattering object under consideration is large in terms of wavelength. In general, a modern high-speed aircraft is quite large electrically and complex in shape. To be able to obtain an accurate radiation pattern, one must take the various scattering structures into account. Based on its applications to previous on-aircraft antenna studies [1-6], the GTD has proven itself well suited to this type of analytical study. Not only does this approach fit nicely into a ray optics format, but it also provides a means of analyzing the effects of three dimensional structures and identifying the significant contributions in the resulting antenna pattern.

Previous GTD solutions for far-field calculations have been shown to be accurate in predicting radiation patterns when compared with various model measurements. However, a significant problem exists with attempting to take far field pattern measurements. In order to satisfy the far-field requirement, one should separate the transmitter and receiver by a minimum distance (i.e., $2D^2/\lambda$, where D is the maximum dimension of the aircraft). Using this requirement for various scale models that have been considered, one would need a range on the order of hundreds to thousands of feet in length. It is obvious, then, that this requirement can not be met for the majority of ranges. The discrepancy caused by the near field measurement is in the definition of directions. That is, the direction from the antenna to the receiver is not the same as that from the center of the aircraft to the receiver. These directions are identical in the far field. Consequently, real far field measured data for most airborne antennas are not practical. In fact from a measurement point of view, it is most advantageous to measure patterns in the extreme near field of the aircraft using a small indoor range and a scale model aircraft. For full scale measurements, it is most convenient to make measurements of the field in the vicinity of the aircraft while the aircraft sits on the flight line. Unfortunately, the near field pattern, that is most easily measured, is not simply related to the far-ield pattern. Therefore, a near field analysis for the air-borne antennas must be carried out.

It should be noted that the GTD solution for the near- and far-field analysis are simply related. Thus the concept of decomposing the aircraft structure into simpler components based on previous analyses [1-6] in the far-field problems is still applicable in the near-field case. As a first step to study the near zone aircraft problem, in this report an analytic solution for the near-zone radiation from a general elliptic cylinder is developed. Section II presents the high frequency asymptotic analysis for slot antennas radiating from a circular cylinder. The results obtained in Section II are then generalized, on the basis of locality of high frequency propagation, to elliptic cylinder problems in Section III. Finally, in Section IV, numerical results calculated from the solution are presented in graphical form and compared with eigenfunction solutions. Excellent agreement is obtained.

II. NEAR ZONE FIELDS EXCITED BY SHORT SLOTS ON LARGE CIRCULAR CYLINDERS

Consider the radiation from a short slot antenna mounted on a perfectly-conducting circular cylinder where the surrounding medium is free space. Figure 1 illustrates the geometry of the problem, where the antenna is located at Q' and the field point at P. According to geometrical optics the region exterior to the cylinder with the antenna at Q' is divided into an illuminated region and a shadowed region by a plane tangent to the cylinder surface at Q'. The plane is referred to as the shadow boundary. A portion of these two regions adjacent to the shadow boundary is a transition region. Previous work (e.g., [7]) based on the Geometrical Theory of Diffraction (GTD) formulation for the fields radiated from an antenna on a cylinder employs three different expressions for the fields in the various regions. Namely, the geometric-optics (GO) solution is used in the "deep" illuminated region, the creeping-wave representation in terms of the residue series in the deep shadow region, and integral representation in terms of Fock functions within the transition region. One then has to "blend" these different representations for the solution to obtain the total field pattern over the entire region exterior to the cylinder. In practical applications, this is accomplished by graphical extrapolation of the solution obtained using different representations until they intersect smoothly in the region where the solution switches from one representation to the other. In this report integral representations in terms of Fock functions are employed throughout the whole space. The integral representation used in the entire illuminated region recovers the GO solution in the "deep" illuminated region, and the integral representation used in the shadow region reduces to the creeping-wave (residue) series representation in the deep shadow region. The following sections will describe how the high-frequency near-zone radiated field may be calculated in the illuminated and shadow regions. The case for the field point P located in the shadow region will be investigated first.

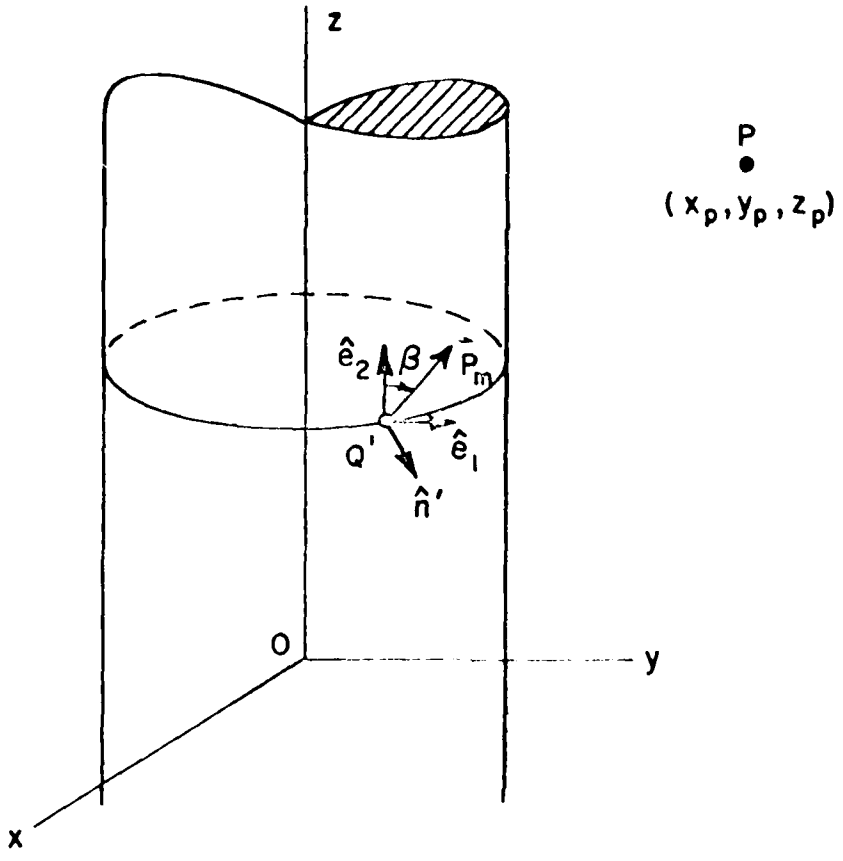

Figure 1. Geometry of the problem considered.

A. Shadow Region

Consider an infinitesimal magnetic current moment $\vec{p}_m$ located on the surface of a circular cylinder at Q' as shown in Figure 2. The field point P is inside the shadow region. The magnetic current moment p_m is arbitrarily oriented and may be resolved into two orthogonal components in terms of the two principle unit tangent vectors e_1 and e_2 of the cylinder surface at Q' (see Figure 1). Thus an arbitrarily oriented magnetic current moment can be resolved into two orthogonal components

$$\vec{p}_m = \hat{e}_1 \, p_m^c \sin \beta + \hat{e}_2 \, p_m^a \cos \beta \, , \tag{1}$$

where β is the angle between $\hat{e}_2$ and $\vec{p}_m$ as shown in Figure 1. In the above expression p_m^c and p_m^a are the equivalent magnetic current moments

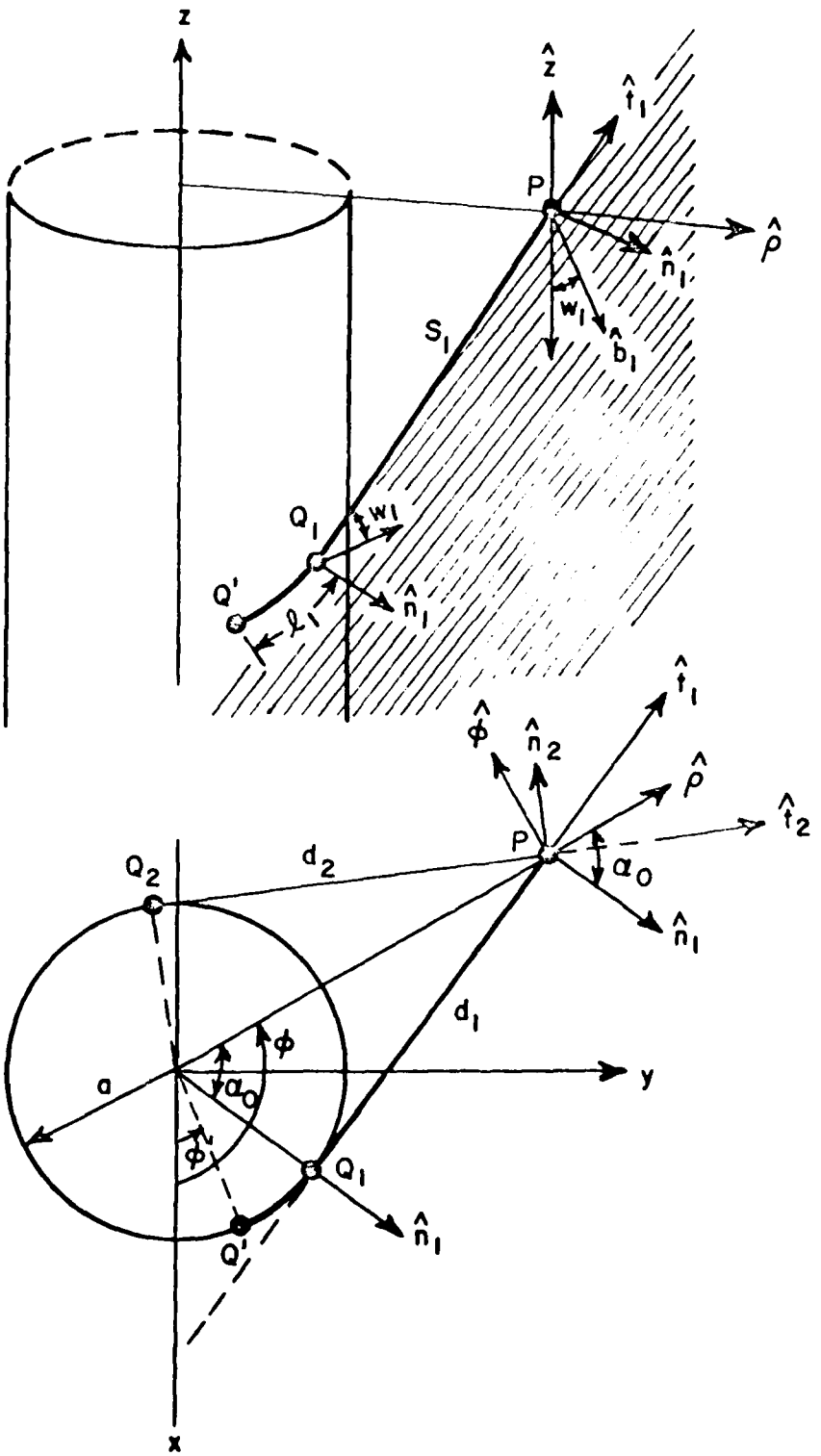

Figure 2. Ray geometry relevant for the analysis in the shadow region.

corresponding to a short circumferential and an axial slot antenna on the cylinder surface. Therefore, to represent the radiation due to a short slot of any orientation, it is sufficient to determine the expressions for short, axial and circumferential slots mounted on a cylinder. It is well known [8] that for a short slot located at Q' (a,ϕ',z') on the circular cylinder with radius a, the formal solution of the fields external to the cylinder at $P(\rho,\phi,z)$ can be expressed as:

$$E_z^a = 0 \tag{2}$$

$$E_\rho^a = \frac{p_m^a}{4\pi^2 a} \int_{-\infty}^{\infty} e^{-jh(z-z')} \frac{1}{\beta\rho} \sum_{n=-\infty}^{\infty} (jn) e^{-jn(\phi-\phi')} \frac{H_n(\beta\rho)}{H_n'(\beta a)} \, dh \tag{3}$$

$$E_\phi^a = \frac{p_m^a}{4\pi^2 a} \int_{-\infty}^{\infty} e^{-jh(z-z')} \sum_{n=-\infty}^{\infty} e^{-jn(\phi-\phi')} \frac{H_n'(\beta\rho)}{H_n'(\beta a)} \, dh \tag{4}$$

$$E_z^c = \frac{p_m^c}{4\pi^2 a} \int_{-\infty}^{\infty} e^{-jh(z-z')} \sum_{n=-\infty}^{\infty} e^{-jn(\phi-\phi')} \frac{H_n(\beta\rho)}{H_n(\beta a)} \, dh \tag{5}$$

$$E_\rho^c = \frac{p_m^c}{4\pi^2 a} \int_{-\infty}^{\infty} e^{-jh(z-z')} \left(\frac{-jh}{\beta}\right) \sum_{n=-\infty}^{\infty} e^{-jn(\phi-\phi')} \frac{H_n'(\beta\rho)}{H_n(\beta a)} \, dh \tag{6}$$

$$- \frac{p_m^c}{4\pi^2 a} \int_{-\infty}^{\infty} e^{-jh(z-z')} \left(\frac{h}{\beta} \frac{1}{\beta a} \frac{1}{\beta\rho}\right) \sum_{n=-\infty}^{\infty} (jn^2) e^{-jn(\phi-\phi')} \frac{H_n(\beta\rho)}{H_n'(\beta a)} \, dh$$

$$E_\phi^c = \frac{p_m^c}{4\pi^2 a} \int_{-\infty}^{\infty} e^{-jh(z-z')} \left(\frac{h}{\beta} \frac{1}{\beta a} \right) \sum_{n=-\infty}^{\infty} n\, e^{-jn(\cdot-\cdot')} \frac{H_n'(\beta\rho)}{H_n'(\beta a)}\, dh \qquad (7)$$

$$- \frac{p_m^c}{4\pi^2 a} \int_{-\infty}^{\infty} e^{-jh(z-z')} \left(\frac{h}{\beta} \frac{1}{\beta\rho} \right) \sum_{n=-\infty}^{\infty} n\, e^{-jn(\cdot-\cdot')} \frac{H_n(\beta\rho)}{H_n(\beta a)}\, dh$$

where

$$\beta^2 = k^2 - h^2.$$

The time dependence $e^{j\omega t}$ and the superscript for the Hankel function of the second kind $H_n^{(2)}(\cdot)$ are understood and suppressed. In the above expressions, E^a and E^c are the fields due to an axial and a circumferential slot radiating from a circular cylinder, respectively. The above formal solutions can not be evaluated exactly. However, for a large radius cylinder and when the field point P is not too close to the cylinder surface (i.e., not inside the paraxial region), the above integrals can be asymptotically evaluated. Following the procedure described in Appendix I, the high frequency asymptotic approximation (keeping only the leading term) for the exact integrals can be expressed as:

$$E_z^a = 0 \qquad (8)$$

$$E_\rho^a \approx \sum_{q=1}^{2} (-1)^{q-1} \left(j \frac{p_m^a}{2} \right) \cos\alpha_o \cos w_q\, g(\xi_q)\, F(\rho_q, s_q) \qquad (9)$$

$$E_\phi^a \approx \sum_{q=1}^{2} \left(-j \frac{p_m^a}{2} \right) \sin\alpha_o \cos w_q\, g(\xi_q)\, F(\rho_q, s_q) \qquad (10)$$

$$E_z^c \approx \sum_{q=1}^{2} \left(j \frac{p_m^c}{2} \right) \cos w_q \left\{ -j \left(\frac{2}{ka \cos w_q} \right)^{1/3} \hat{g}(\xi_q) \right\} F(\rho_q, s_q) \qquad (11)$$

$$E_\phi^c \approx \sum_{q=1}^{2} \left(-j \frac{p_m^c}{2}\right) \sin\alpha_o \sin w_q \left\{-j\left(ka \cos w_q\right)^{1/3} \tilde{g}(\xi_q)\right\} F(\ell_q, s_q)$$

$$+ \sum_{q=1}^{2} \left(-j \frac{p_m^c}{2}\right) \cos\alpha_o \sin w_q \, g(\xi_q) \, F(\ell_q, s_q) \qquad (12)$$

$$E_\theta^c \approx \sum_{q=1}^{2} (-1)^{q-1} \left(j \frac{p_m^c}{2}\right) \sin\alpha_o \sin w_q \, g(\xi_q) \, F(\ell_q, s_q)$$

$$+ \sum_{q=1}^{2} (-1)^{q-1} \left(-j \frac{p_m^c}{2}\right) \cos\alpha_o \sin w_q \left\{-j\left(ka \cos w_q\right)^{1/3} \tilde{g}(\xi_q)\right\} F(\ell_q, s_q) \qquad (13)$$

where

$$F(\ell_q, s_q) = \frac{e^{-jk\ell_q} e^{-jk s_q}}{\sqrt{s_q(s_q + \ell_q)}}, \qquad (14)$$

$$\xi_1 = \left(\frac{ka \cos w_1}{2}\right)^{1/3} (|\phi - \phi'| - \alpha_o) \qquad (15)$$

and

$$\xi_2 = \left(\frac{ka \cos w_2}{2}\right)^{1/3} (2\pi - |\phi - \phi'| - \alpha_o). \qquad (16)$$

In the above expressions, $g(\cdot)$ and $\tilde{g}(\cdot)$ are the well-tabulated Fock functions [9], and the parameters α_o, w_q, ℓ_q and s_q are defined in Appendix I. These vector components of the electric field can be cast

into a ray format in that two orthogonal field components (transverse to the ray path) travel from the source point Q', along the geodesic, to the field point P. This will be described in the following sections.

First, let us introduce several parameters. According to the generalized Fermat's principle proposed by Keller [10], contribution of $\vec{E}$ at P is the field on the ray from Q' to Q_1 (which is the geodesic on the conducting surface), then from Q_1 to P which is a straight line tangent to the surface at Q_1 (see Figure 2). The unit tangent, normal, and binormal vectors of the ray are $(\hat{t}_1, \hat{n}_1, \hat{b}_1=\hat{t}_1 x \hat{n}_1)$ at Q_1. Note that $(\hat{t}_1, \hat{n}_1, \hat{b}_1)$ form a moving trihedron along the straight path from Q_1 to P. The vector components in terms of the cylindrical coordinate system $(\cdot,\cdot,z)$ can be cast into the vector components in the ray coordinate system (t,n,b). Equations (8)-(13), therefore, can be easily expressed in the ray coordinate system as follows:

$$\vec{E}^a_n \approx j \frac{p^a_m}{2} [\cos w_1 \, g(\xi_1) \, F(\ell_1, s_1)\hat{n}_1$$

$$- \cos w_2 \, g(\xi_2) \, F(\ell_2, s_2)\hat{n}_2] \tag{17}$$

$$\vec{E}^a_b = 0 \tag{18}$$

$$\vec{E}^c_n \approx -j \frac{p^c_m}{2} \{\sin w_1 \, g(\xi_1) \, F(\ell_1, s_1)\hat{n}_1$$

$$+ \sin w_2 \, g(\xi_2) \, F(\ell_2, s_2)\hat{n}_2\} \tag{19}$$

$$\vec{E}^c_b \approx -j \frac{p^c_m}{2} \left\{-j\left(\frac{2}{ka \cos w_1}\right)^{1/3} \tilde{g}(\xi_1) \, F(\ell_1, s_1)\hat{b}_1 \right. \tag{20}$$

$$\left. +j\left(\frac{2}{ka \cos w_2}\right)^{1/3} \tilde{g}(\xi_2) \, F(\ell_2, s_2)\hat{b}_2 \right\}$$

note that $\hat{n}_1$ is the unit normal vector at Q_1, $\hat{t}_1$ is the unit vector directeddfrom Q_1 toward P, and $\hat{b}_1 = \hat{t}_1 \times \hat{n}_1$. Similar definitions are used for $(\hat{t}_2, \hat{n}_2, \hat{b}_2)$. It is interesting to note that only field components transverse to the ray exist in the final expressions. Before proceeding to the next section, it should be noted that the final expressions, Equations (17)-(20) are approximate solutions for large radius cylinders with field point not close to the surface. The analysis for the field point close to the surface has to be carried out differently.

B. Illuminated Region

If the field point P is in the illuminated region as shown in Figure 3, the radiation from the source Q' on the circular cylinder propagates along a straight line to P. According to geometrical optics, the electric field at P due to a short magnetic current moment $\vec{p}_m$ defined by Equation (1) at Q' can be expressed

$$\vec{E}^a_{\phi'} = -jp^a_m \sin\theta' \frac{e^{-jks}}{s} \hat{\phi}' \tag{21}$$

$$\vec{E}^c_{\phi'} = jp^c_m \cos\theta' (\hat{e}_1 \cdot \hat{t}) \frac{e^{-jks}}{s} \hat{\phi}' \tag{22}$$

$$\vec{E}^c_{\theta'} = -jp^c_m (\hat{n}' \cdot \hat{t}) \frac{e^{-jks}}{s} \hat{\theta}' \tag{23}$$

where $\hat{n}'$ is the unit normal vector at Q', $\vec{s}$ is the vector directed from Q' toward P, and $(\hat{\theta}', \hat{\phi}')$ are the local ray coordinate systems as shown in Figure 3. Note that $\hat{e}_1 \cdot \hat{t} = (\hat{e}_1 \cdot \hat{s})/\sin\theta'$ and $\hat{n}' \cdot \hat{t} = (\hat{n}' \cdot \hat{s}) \sin\theta'$.

Using a heuristic approach, Ivanov [11] employed a parabolic equation method to find the asymptotic behavior of the current in the illuminated side of the cylinder due to a plane wave illumination. Ivanov's solution, employing an integral representation in terms of Fock functions, is valid in the illuminated region and holds right up to the shadow boundary. Furthermore, his solution, when applied in the "deep" illuminated region, has the same accuracy as the first two terms of the asymptotic form of the geometrical optics solution. Based on this observation, together with the reciprocity theorem and the similitude concept [12], Ivanov's result is employed to modify the geometrical optics solution given by

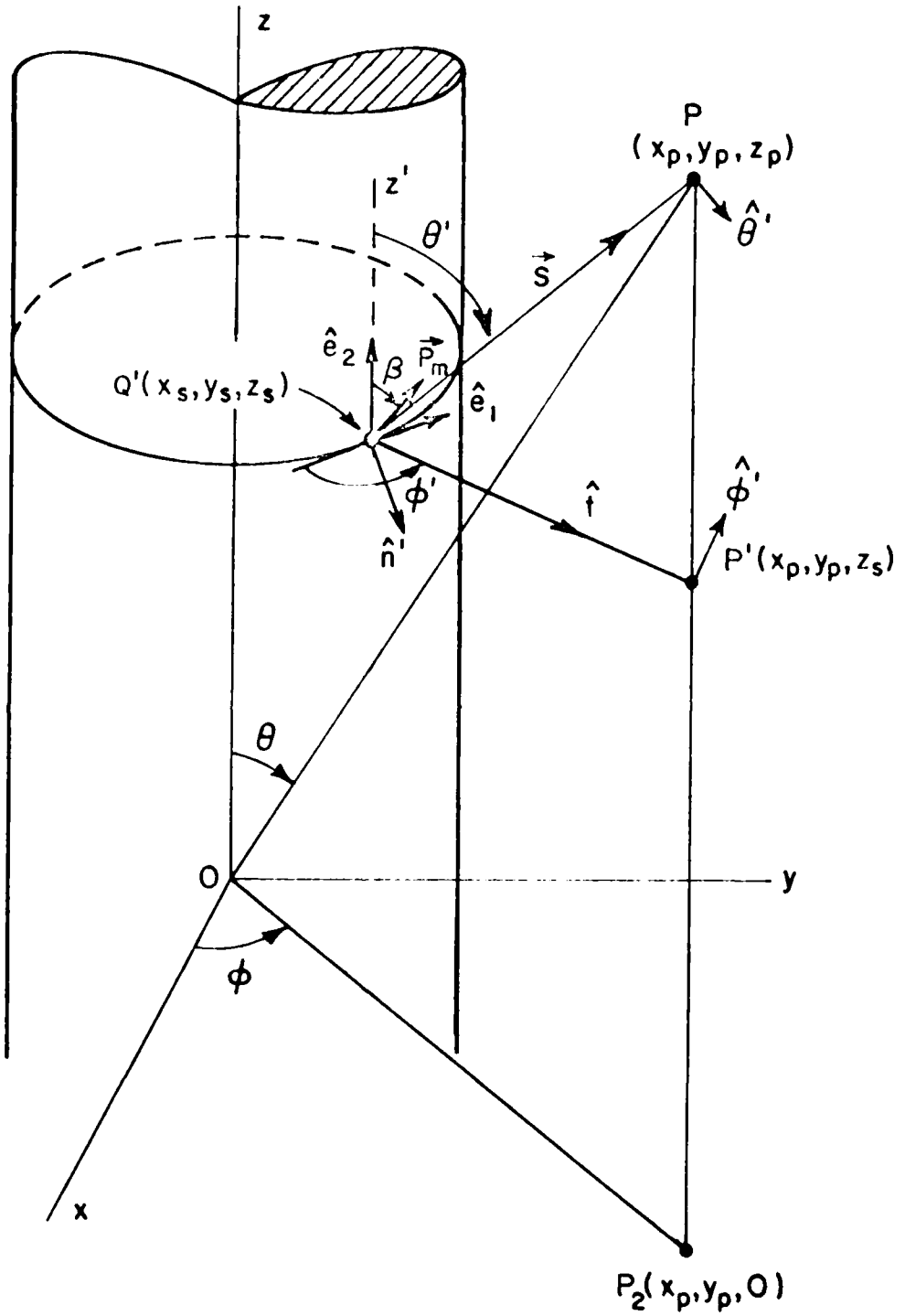

Figure 3. Geometry relevant for the analysis in the illuminated region.

Equations (21) to (23). The final expression for the electric field at P inside the illuminated region due to short slots on a circular cylinder can be written as:

$$\vec{E}^a_{\phi'} \approx -j \frac{p^a_m}{2} \sin\theta' \, G(\xi^{lit}) \, \frac{e^{-jks}}{s} \, \hat{\phi}' \tag{24}$$

$$\vec{E}^c_{\phi'} \approx j \frac{p^c_m}{2} \cos\theta' \, (\hat{e}_1 \cdot \hat{t}) \, G(\xi^{lit}) \, \frac{e^{-jks}}{s} \, \hat{\phi}' \tag{25}$$

$$\vec{E}^c_{\theta'} \approx -j \frac{p^c_m}{2} \left\{ -j \left(ka \frac{2}{\sin\theta'} \right)^{1/3} \tilde{G}(\xi^{lit}) \right\} \frac{e^{-jks}}{s} \, \hat{\theta}' \tag{26}$$

where

$$\xi^{lit} = -\left(\frac{ka \sin\theta'}{2} \right)^{1/3} (\hat{n}' \cdot \hat{t}) \, . \tag{27}$$

The functions $G(\cdot)$ and $\tilde{G}(\cdot)$ are related to the Fock functions $g(\cdot)$ and $\tilde{g}(\cdot)$ by the following equations:

$$G(x) = e^{-jx^3/3} \, g(x) \tag{28}$$

and

$$\tilde{G}(x) = e^{-jx^3/3} \, \tilde{g}(x) \tag{29}$$

It should be emphasized that the above Equations (24) to (27) are obtained via an engineering approach. This is accomplished by combining Ivanov's result and the geometric optics solution for a magnetic current moment located on a large circular cylinder. However, numerical results obtained by using Equations (24) to (27) show excellent agreement with the eigenfunction solution for the same problem (see Section IV), thereby confirming their validity.

III. GTD GENERALIZATION FROM CIRCULAR CYLINDER TO GENERAL ELLIPTIC CYLINDERS

The high frequency asymptotic solutions obtained for fields radiated from slot antennas on a circular cylinder will now be generalized, on the basis of locality of the high frequency propagation, to the elliptic cylinder problem. The case for the field point P located in the illuminated region will be investigated first.

A. Illuminated Region

Consider a slot antenna radiating from the surface of an elliptic cylinder with radius of curvature ρ_τ.

Based on the local nature of high frequency radiation from slot on cylinder, the results obtained in the previous sections for the circular cylinder problem can be directly applied to the elliptic cylinder case. Specifically, Equations (24) through (27) can be modified for the elliptic cylinder case by replacing the radius of the circular cylinder "a" by the cross sectional radius of curvature $\rho_\tau(Q')$ of the ellipse at the source location Q'. Thus, the fields of slot antennas radiating from an elliptic cylinder can be expressed as:

$$\vec{E}^a_{\phi'} \approx -j \frac{p^a_m}{2} \sin\theta' \, G(\xi^{lit}) \frac{e^{-jks}}{s} \hat{\phi}' \tag{30}$$

$$\vec{E}^c_{\phi'} \approx j \frac{p^c_m}{2} \cos\theta' \, (\hat{e}_1 \cdot \hat{t}) \, G(\xi^{lit}) \frac{e^{jks}}{s} \hat{\phi}' \tag{31}$$

$$\vec{E}^c_{\theta'} \approx -j \frac{p^c_m}{2} \left\{ -j \left(\frac{2}{k\rho_\tau(Q')\sin\theta'} \right)^{1/3} \right\} \hat{G}(\xi^{lit}) \frac{e^{-jks}}{s} \hat{\theta}' \tag{32}$$

where

$$\xi^{lit} = -\left(\frac{k\rho_\tau(Q')\sin\theta'}{2} \right)^{1/3} (\hat{n}' \cdot \hat{t}) \tag{33}$$

The parameters in the above equations have the same definition as those in Equations (24) thorugh (27). This concludes the analysis in the illuminated region.

B. Shadow Region

In this section, radiation from an elliptic cylinder where the field point is located in the shadow region is considered. Again, the solution obtained for the circular cylinder problem is generalized to the elliptic cylinder case based on the locality of high frequency propagation. One assumes that the radiation from a cylinder of general elliptic cross section may be described in terms of rather highly attenuated surface waves originating in the neighborhood of the source and traveling around the cylinder in opposite directions. For the circular cylinder, each of these waves is represented by a decaying amplitude and a phase that increases essentially linearly with distance along the geodesic. Referring to Equations (17) through (20), one notes that the variation of the surface wave is essentially described by the factor $e^{-jk\ell} g(\xi)$, where ℓ is the distance traveled along geodesic path on the surface and ξ is related to ℓ. The parameter ξ given by Equations (15) and (16) is examined to identify this relation. Equation (15)

$$\xi_1 = \left(\frac{ka \cos w_1}{2}\right)^{1/3} (|\phi-\phi'|-\alpha_o)$$

can be written in a different form:

$$\xi_1 = \left[\frac{k}{2\rho_g^2}\right]^{1/3} \ell_1 \tag{34}$$

where $\rho_g = a/\cos^2 w_1$ can be identified to be the radius of curvature along the geodisic path, and $\ell_1 = a(|\phi-\phi'|-\alpha_o)/\cos w_1$ is indeed the arc length along the geodesic. It follows from the work of Fock [13], Wetzel [14], and Goodrich [15] that the procedure on an elliptic cylinder is to divide the surface into small segments over each of which the radius of curvature may be considered approximately constant. The variation of the surface wave over each segment is calculated as if the segment were a section of a circular cylinder with a radius equal to the local radius of curvature. The total variation in the surface wave is taken to be the sum of the increments so calculated. Thus the near-zone fields, Equations (17) through (20), of slot antenna radiating from a circular cylinder can now be generalized for the elliptic cylinder case:

$$\vec{E}_n^a \approx j \frac{p_m^a}{2} \left\{ \cos w_1\, g(\xi_1) \left(\frac{\rho_g(Q_1)}{\rho_g(Q')}\right)^{1/6} F(\ell_1, s_1)\hat{n}_1 \right. \tag{35}$$

$$\left. -\cos w_2\, g(\xi_2) \left(\frac{\rho_g(Q_2)}{\rho_g(Q')}\right)^{1/6} F(\ell_2, s_2)\hat{n}_2 \right\}$$

$$\vec{E}_b^a = 0 \tag{36}$$

$$\vec{E}_n^c \approx -j \frac{p_m^c}{2} \left\{ \sin w_1 \; g(\xi_1) \left(\frac{\rho_g(Q_1)}{\rho_g(Q')} \right)^{1/6} F(\xi_1, s_1) \; n_1 \right. \tag{37}$$

$$\left. + \sin w_2 \; g(\xi_2) \left(\frac{\rho_g(Q_2)}{\rho_g(Q')} \right)^{1/6} F(\xi_2, s_2) n_2 \right\}$$

$$\vec{E}_b^c \approx -j \frac{p_m^c}{2} \left\{ -j \left(\frac{2}{k\rho_\tau(Q')\cos w_1} \right)^{1/3} \tilde{g}(\xi_1) \left(\frac{\rho_g(Q_1)}{\rho_g(Q')} \right)^{1/6} F(\xi_1 s_1) b_1 \right. \tag{38}$$

$$\left. + j \left(\frac{2}{k\rho_\tau(Q')\cos w_2} \right)^{1/3} \tilde{g}(\xi_2) \left(\frac{\rho_g(Q_2)}{\rho_g(Q')} \right)^{1/6} F(\xi_2, s_2) b_2 \right\}$$

where

$$\xi_i = \int_{Q'}^{Q_i} \left[\frac{2}{k\rho_g^2} \right]^{1/3} d\ell_i \tag{39}$$

where the integration is performed along the geodesic from the source Q' to the diffraction point Q_i. The additional factor

$$\left(\frac{\rho_g(Q_i)}{\rho_g(Q')} \right)^{1/6}$$

must be incorporated in the generalization to the general elliptic cylinder to preserve reciprocity and to reduce uniformly to Keller's surface ray field in the deep shadow region [16] as indicated in [7]; it is observed that this factor also occurs in a result given by Logan and Yee [17] which is based on a more complicated boundary layer method of solution. This concludes the analysis of the solution for the near zone field due to axial and circumferential slots radiating from an elliptic cylinder.

For an arbitrarily oriented slot $\vec{p}_m$ defined by Equation (1), the total field can be readily obtained via the superposition theorem:

$$E_n = \sin \psi\, E_n^c + \cos \psi\, E_n^a \tag{40}$$

$$E_b = \sin \psi\, E_b^c + \cos \psi\, E_b^a. \tag{41}$$

Note that it is straightforward to transform the field solutions given in Sections III and IV into the spherical coordinate systems (r,θ,ϕ) defined in Figure 3.

IV. NUMERICAL RESULTS

In this section various numerical results obtained by using the equations described in the previous sections are presented for slot antennas radiating from a general elliptic cylinder.

Consider a short magnetic current moment $\vec{p}_m = \hat{e}_1 p_m^c \sin \psi + \hat{e}_2 p_m^a \cos \psi$ where $\psi = 45°$ radiating from a circular cylinder. The source is located at Q' on the cylinder with radius "a" with cylindrical coordinate system ($\rho' = a$, $\phi' = 180°$, and $z' = 0$). The field point is located at P with (ρ, ϕ, z). Figures 4 and 5 show the patterns of E_θ and E_ϕ for a field point P located at (ρ, $z = 1000\lambda$) and ϕ varies from 0° to 360°. This is a conical pattern with the cone angle equal to 45°. The far-field conical pattern with $\theta = 45°$ is also calculated using eigenfunction series and plotted in Figures 4 and 5. It is observed in Figure 4 that E_θ calculated from the high frequency asymptotic solutions at $\rho = 1000\lambda$ agrees very well with the far-zone eigenfunction solution. The field component E_ϕ as shown in Figure 5 also shows excellent agreement between the two solutions except for $240° \leq \phi \leq 330°$. The reason for the disagreement in this small region is that the leading terms of E_ϕ^a and E_ϕ^c given in Equations (17), (19), (24) and (25) almost cancel with each other in that region. This is demonstrated in Figures 6 and 7. Figure 6 is the pattern E_ϕ^c contributed from the circumferential component of the magnetic current moment, and Figure 7 is the pattern E_ϕ^a resulted from the axial component. As described in Appendix I, for this special situation, the next higher order term in the asymptotic solutions is important and should be included. Figure 8 shows the final result when the next higher-order term is included. One observes that the refined solution shows excellent agreement with the eigenfunction result. Next some numerical results for an elliptic cylinder case are presented. Figures 9 and 10 show the radiation patterns E_θ and E_ϕ due to the same 45° magnetic current moment radiating from an elliptic cylinder. The results seem to be reasonable, however, independent checks will be performed later using other solutions (e.g., an integral-equation solution). The results just

shown confirmed the validity of the solution for the far zone calculation (i.e., $\rho=1000\lambda$). However, the solutions are also useful for near zone calculations. Figure 11 presents the result E_{ϕ}^{a} in the principle plane for an axial slot radiating from a circular cylinder (radius a=) with the field point P located at ($\rho=10\lambda$, ϕ, and $z=0$). The exact solution Equation (4) is available but can not be evaluated exactly. However, numerical integration techniques can be employed to obtain approximate results. This is a tedious procedure and will be investigated in the future. In order to check the near zone result, a two dimensional problem, namely, an infinitely-long slot radiating from the circular cylinder, is considered. It is well known that the radiation pattern for a short axial slot in the principal plane is identical to that of a magnetic line source mounted on a cylinder. The eigenfunction result for the two dimensional problem is also plotted in Figure 11. One can see the excellent agreement. For comparison, the far zone eigenfunction result is also included in Figure 11. It is interesting to note that for this case, the near zone pattern retains the shape of the far zone result but the front to back ratio is decreased in the near zone case. Judging from these results, it is believed that the solution obtained in Sections II and III are useful to calculate the near zone field due to short slot antennas with arbitrary orientation radiating from a general elliptic cylinder.

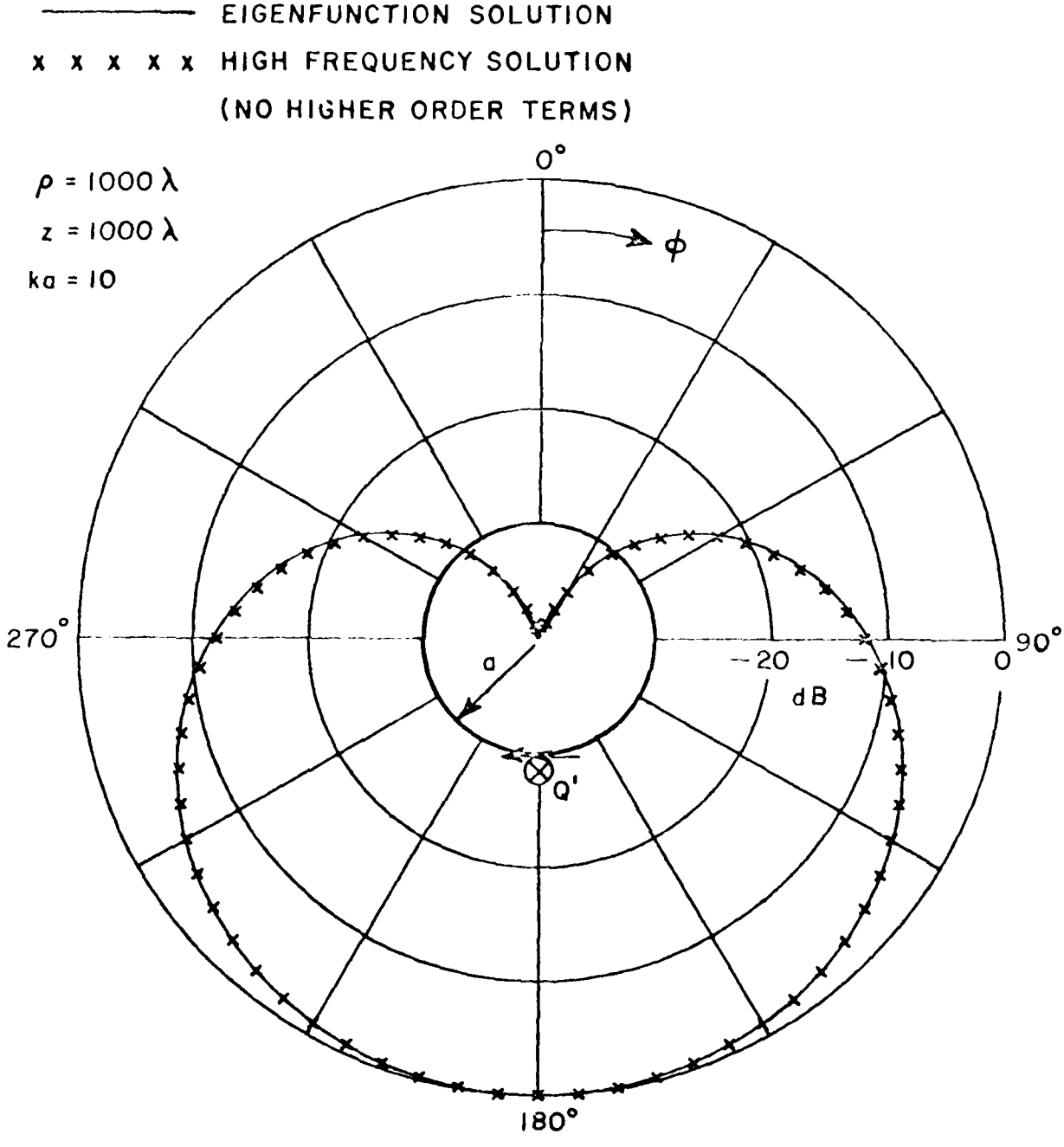

Figure 4. Normalized radiation pattern E_θ due to an orientated slot antenna (β=45°) on a circular cylinder at Q'.

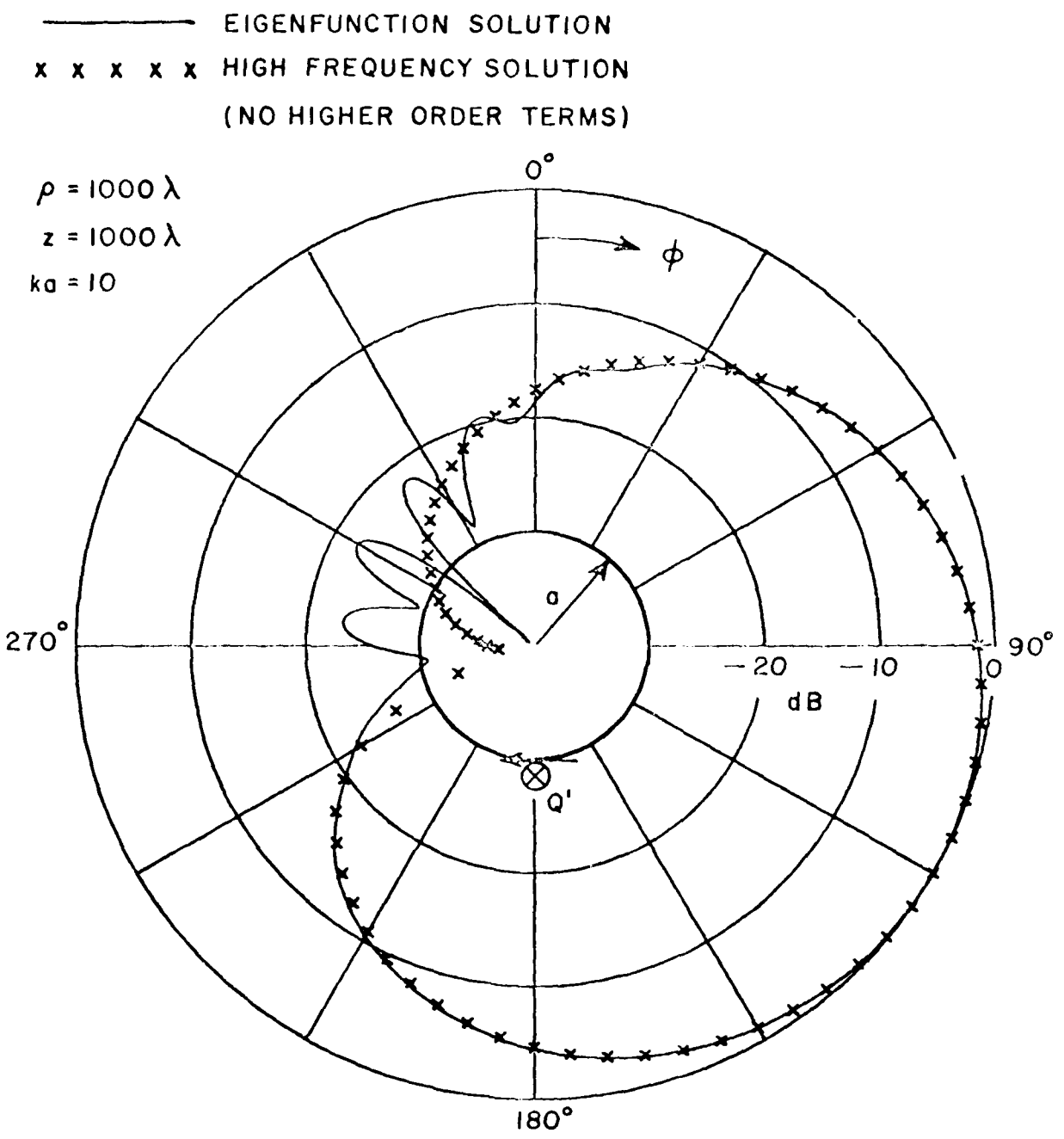

Figure 5. Normalized radiation pattern E_ϕ due to an orientated slot antenna (β=45°) on a circular cylinder at Q'.

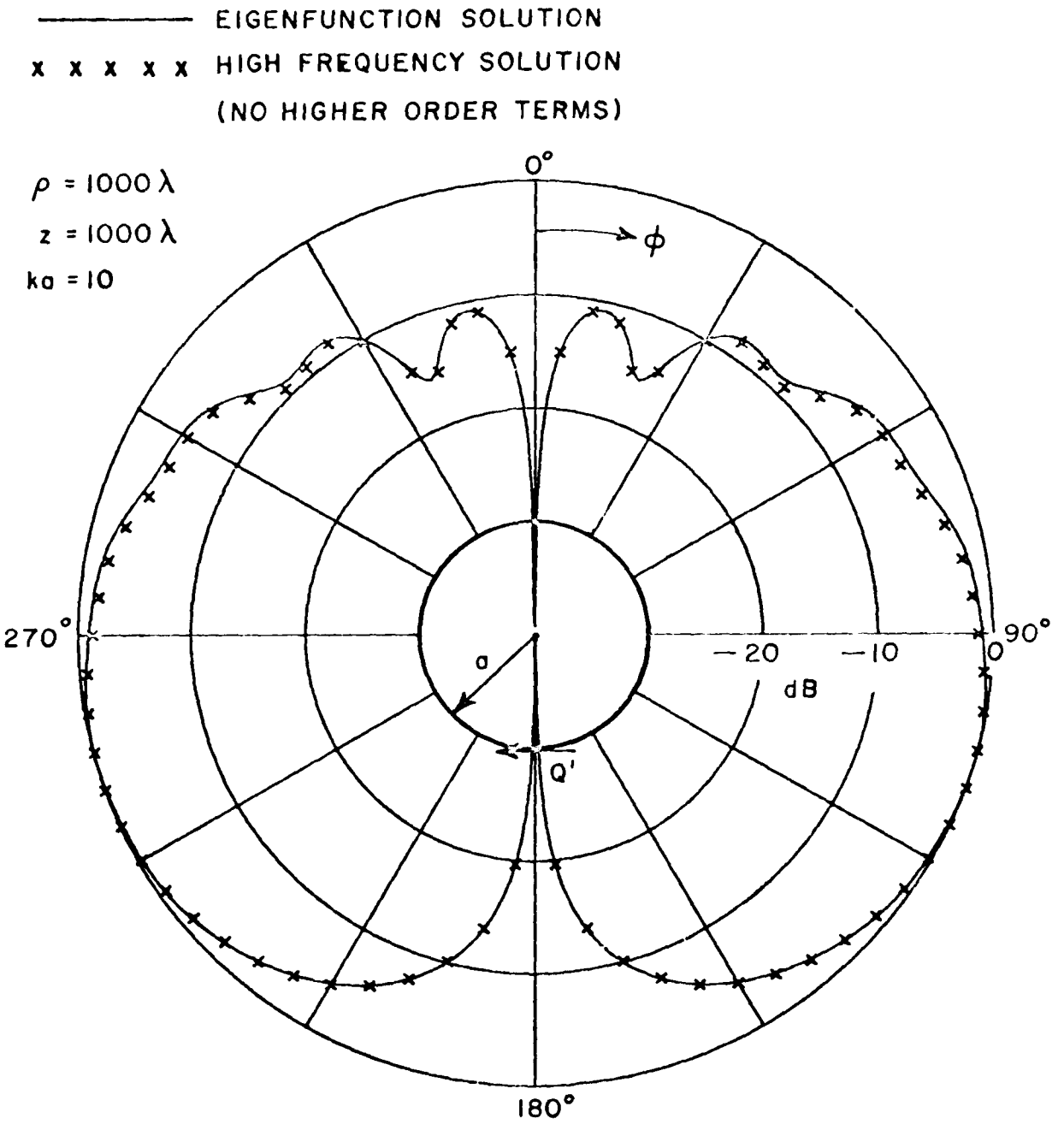

Figure 6. Normalized radiation pattern E_{ϕ}^{c} contributed from the circumferential component p_{m}^{c} of $\vec{p}_{m}$ in Figure 5.

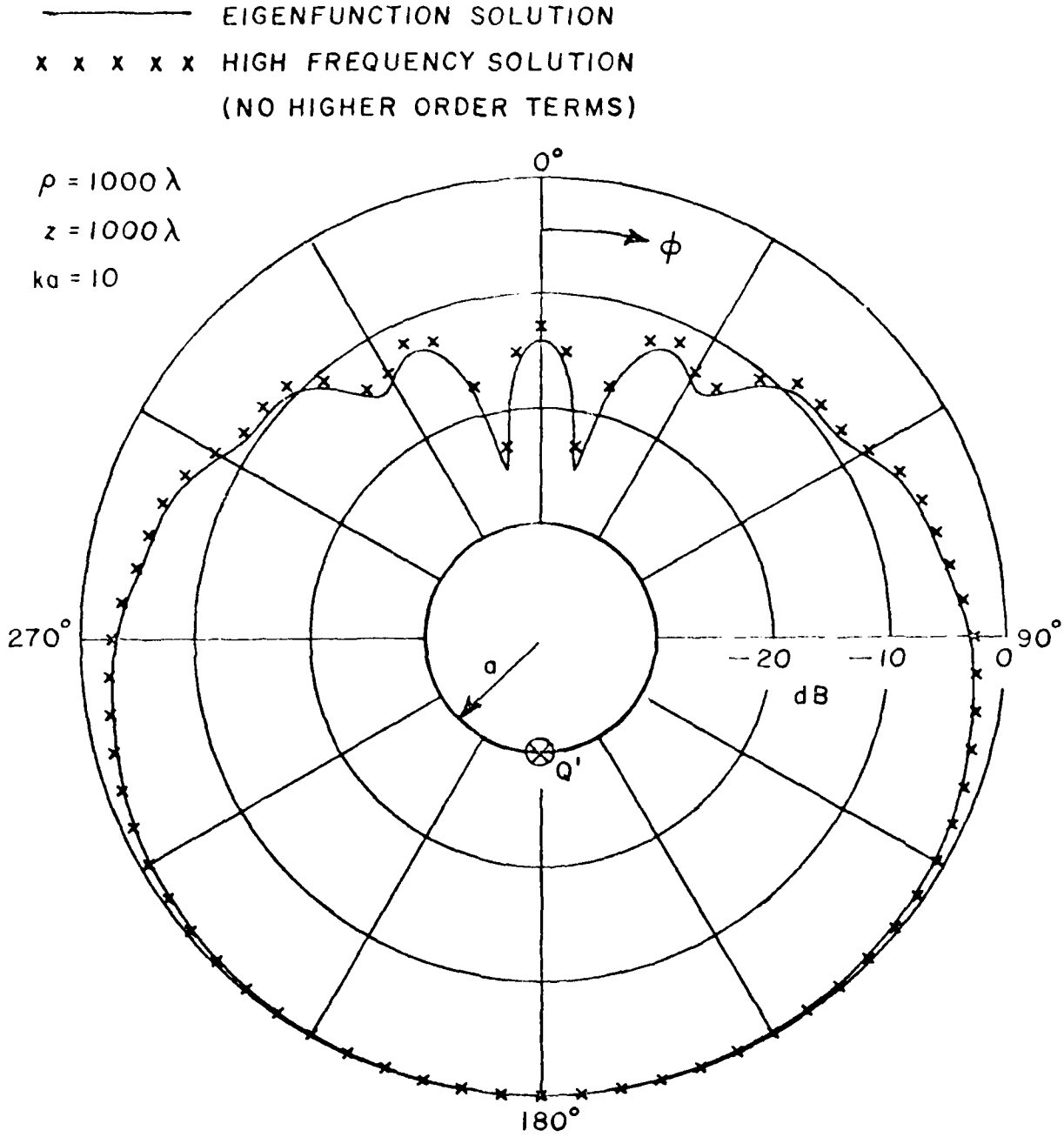

Figure 7. Normalized radiation pattern E_{ϕ}^{a} contributed from the axial component p_m^a of $\vec{p}_m$ in Figure 5.

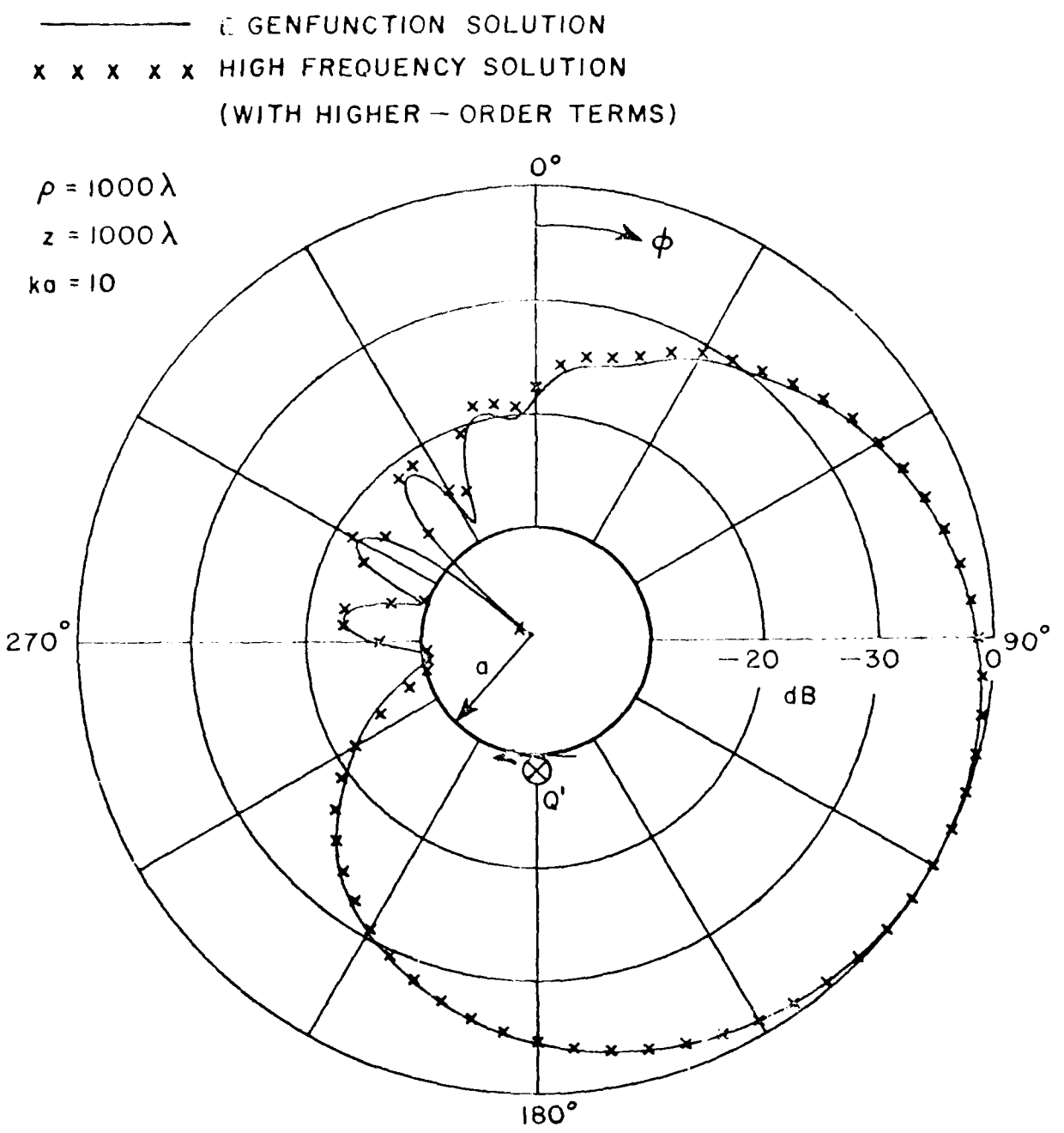

Figure 8. Normalized radiation patterns E_ϕ (with higher order term induced) for the problem considered for Figure 4.

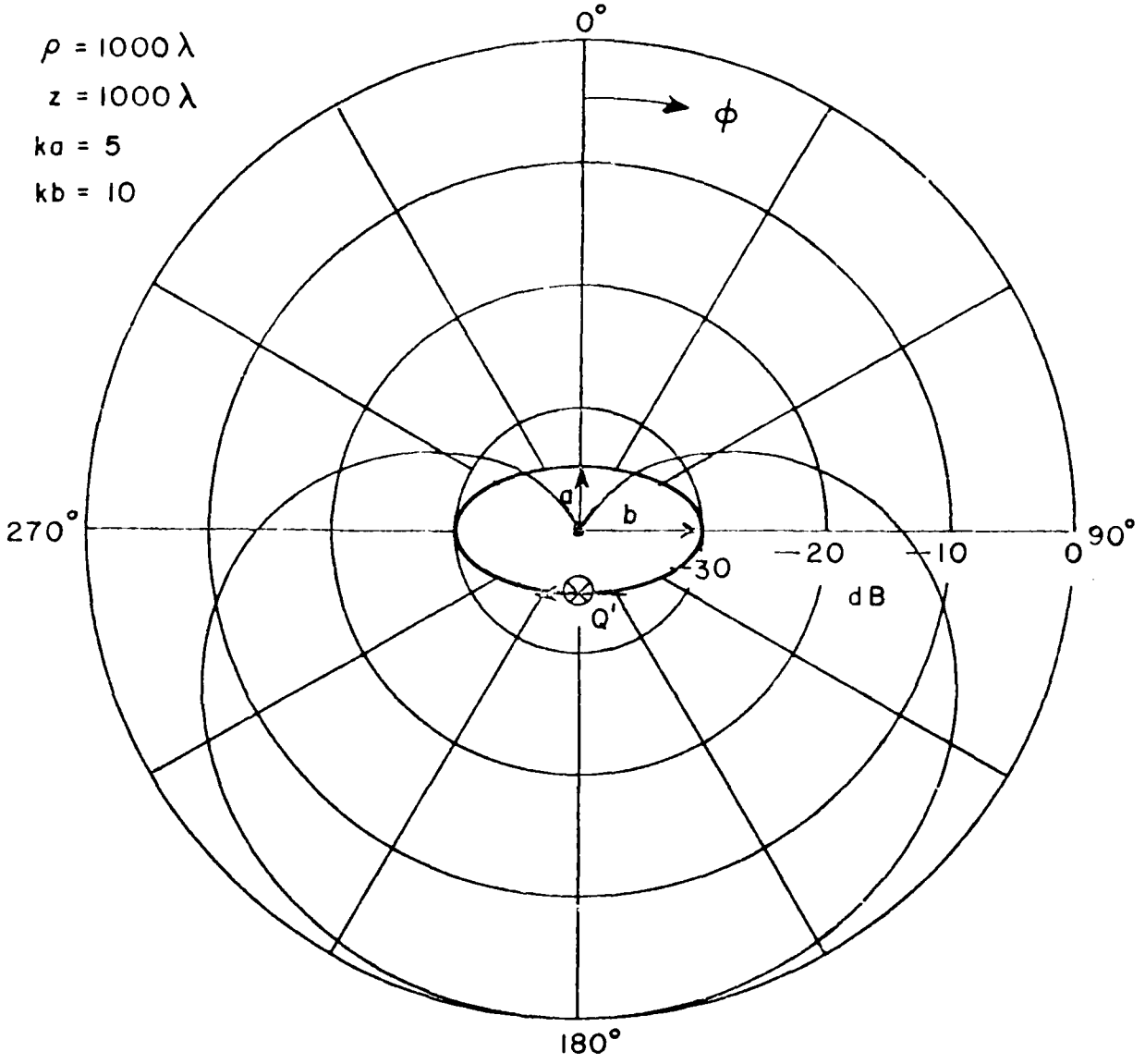

Figure 9. Normalized radiation pattern E_θ due to an orientated slot antenna (β=45°) on an elliptic cylinder.

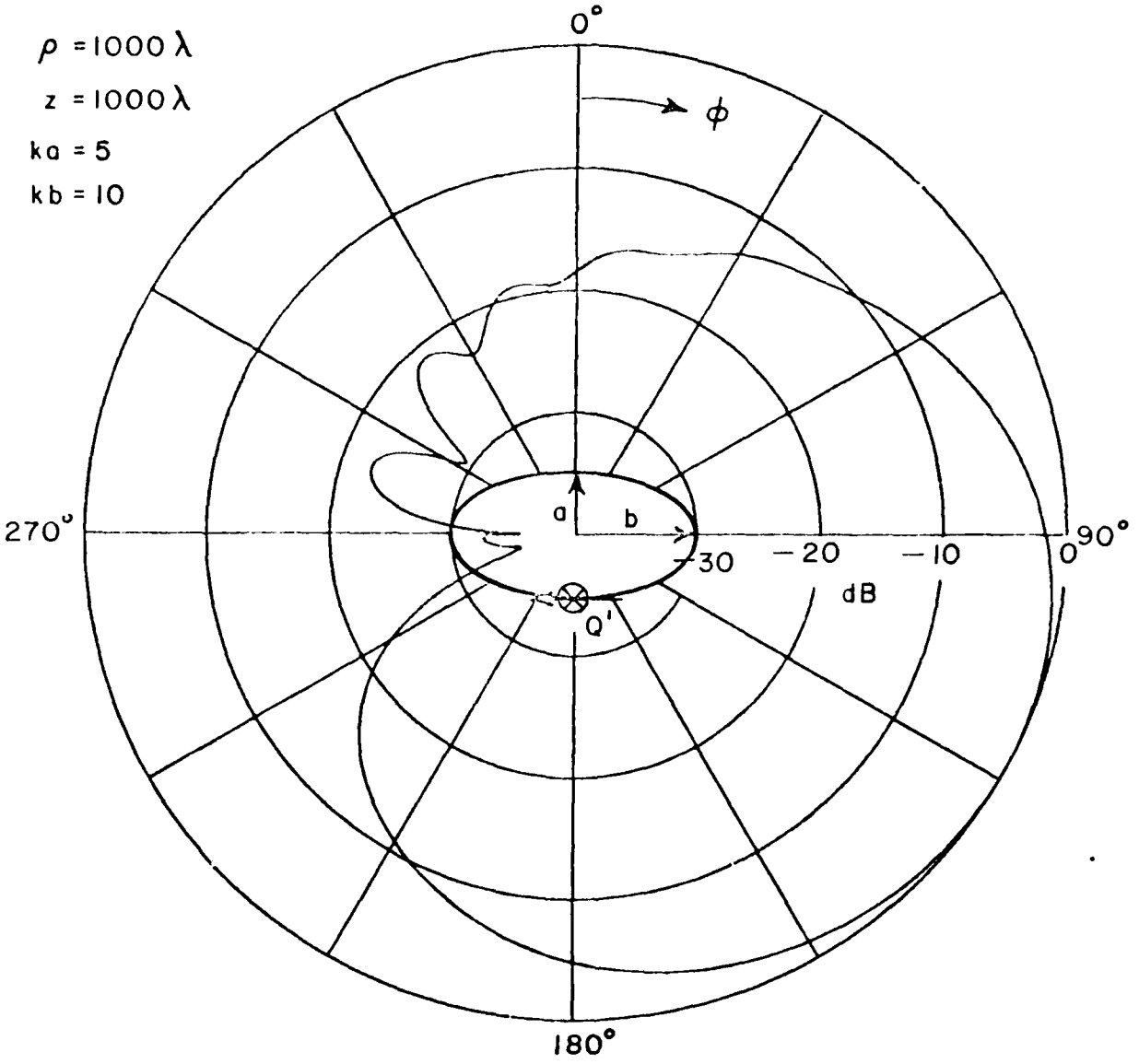

Figure 10. Normalized radiation pattern E_ϕ due to an orientated slot antenna (β=45°) on an elliptic cylinder.

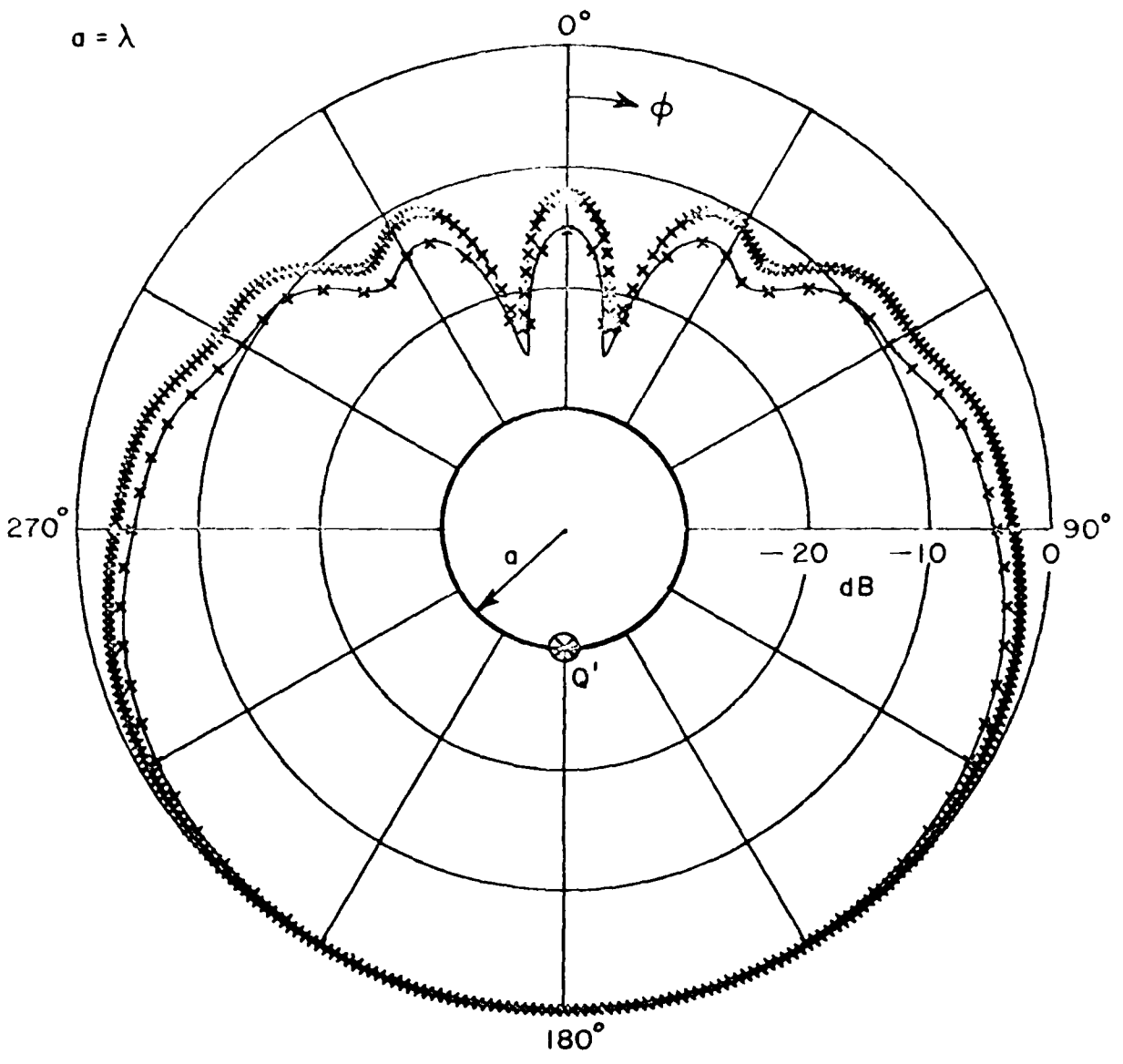

Figure 11. Normalized near zone radiation pattern E_{ϕ}^{a} due to an axial slot antenna on a circular cylinder. (In the principle plane z=0.)

V. SUMMARY

Near zone radiation characteristics for an antenna radiating from a general elliptic cylinder are investigated. Integral representations in terms of Fock functions for the radiated fields are employed throughout the entire space exterior but not close to the cylinder. In the illuminated region, an engineering approach, employing Ivanov's results for the field produced by plane wave reflection at a convex cylinder, is used to derive the expressions for the fields due to slots radiating on circular cylinders. This representation is valid in the illuminated region and holds up to the shadow boundary. Furthermore, this solution, when applied in the "deep" illuminated region, has the same accuracy as the first two terms of the asymptotic form of the geometric optics solution. On the other hand, a high frequency asymptotic solution is derived from the rigorous solution for a slot antenna radiating from a circular cylinder. This solution is, again, an integral representation in terms of the Fock functions. It can be shown that in the deep shadow region this integral representation reduces to the creeping-wave (residue) series representation.

The solution obtained for the circular cylinder problem is then generalized, on the basis of locality of high frequency propagation, to the general elliptic cylinder case.

The solution described in this report is employed to calculate the near-zone field radiated from a short slot mounted on a general elliptic cylinder. The numerical results thus obtained show excellent agreement with various other solutions when the field point is in the far zone. Our solution is also valid in the near zone, however, it remains a task to generate the near zone results by using other solutions for comparison.

REFERENCES

[1] W. D. Burnside, "Analysis of On-Aircraft Antenna Patterns," Report 3390-1, August 1972, The Ohio State University ElectroScience Laboratory, Department of Electrical Engineering: prepared under Contract N62269-72-C-0354 for Naval Air Development Center. (AD 777 989)

[2] W. D. Burnside, R. J. Marhefka, and C. L. Yu, "Roll Plane Analysis of On-Aircraft Antennas," IEEE Trans. on Antennas and Propagation, Vol. AP-21, November 1973, pp. 780-786.

[3] R. J. Marhefka and W. D. Burnside, "Numerical Solutions to Some On-Aircraft Antenna Pattern Problems," Technical Report 3390-4, October 1973, The Ohio State University ElectroScience Laboratory, Department of Electrical Engineering; prepared under Contract N62269-72-C-0354 for Naval Air Development Center.

[4] W. D. Burnside, M. C. Gilreath, R. J. Marhefka, and C. L. Yu, "A Study of KC-135 Aircraft Antenna Patterns," IEEE Trans. on Antennas and Propagation, Vol. AP-23, No. 3, May 1975, pp. 309-316.

[5] C. L. Yu and W. D. Burnside, "MLS Airborne Antenna Research," Semiannual Report 2902-22, May 1975, The Ohio State University ElectroScience Laboratory, Department of Electrical Engineering; prepared under Grant NGL 36-003-138 for National Aeronautics and Space Administration, Langley Research Center.

[6] C. L. Yu and W. D. Burnside, "Volumetric Pattern Analysis of Fuselage-Mounted Airborne Antennas," Report 2902-24, April 1976, The Ohio State University ElectroScience Laboratory, Department of Electrical Engineering; prepared under Grant Number NGL 36-008-138 for National Aeronautics and Space Administration.

[7] P. H. Pathak and R. G. Kouyoumjian, "An Analysis of the Radiation from Apertures in Curved Surfaces by the Geometrical Theory of Diffraction," Proceedings of the IEEE, Vol. 62, No. 11, November 1974, pp. 1409-1447.

[8] S. Silver and W. K. Saunders," "The Electrical Field Produced by a Slot in an Infinite Circular Cylinder," Journal of Applied Physics, Vol. 21, February 1950, pp. 153-158.

[9] N. A. Logan, "General Research in Diffraction Theory" Missiles and Space Division, Lockheed Aircraft Corp., Vol. 1, Rep. LMSD-288087 and Vol. 2, Rep. LMSD-288088, December 1959.

[10] J. B. Keller, "Geomerical Theory of Diffraciton," J. Opt. Soc. Amer., Vol. 57, No. 2, pp. 116-130, Febraury 1962.

[11] V. I. Ivanov, ""Uniform Asymptotic Behavior of the Field Produced by Plane Wave Reflections at a Convex Cylinder. I," USSR Comput. Math. Phys., Vol. 11, No. 1, January, pp. 216-232.

[12] J. H. Richmond and N. N. Wang, "Scattering by Noncircular Conducting Cylinders with Thin Dielectric Coating," URSI June 1974 meeting, Atlanta, Ga.

[13] V. A. Fock, "Electromagnetic Diffraction and Propagation Problems," New York: Pergamon, 1965.

[14] L. Wetzel, "High Frequency Current Distribuiton on Conducting Obstacles," Cruft Laboratory, Harvard University, Cambridge, Mass. Sci. Rep. 10, 1957.

[15] R. F. Goodrich, et al., "Radiation from Slot Arrays on Cones," IRE Trans. Antennas Propagat., Vol. AP 7, July 1959, pp. 213-222.

[16] J. B. Keller, "Diffraction by a Convex Cylinder," IRE Trans. AP-4, 312-321, 1956.

[17] N. A. Logan and K. S. Yee, "A Mathematical Model for Diffraction by Convex Surfaces," Electromagnetic Waves, edited by R. G. Langer, The University of Wisconsin Press, Madison, 1962.

[18] J. R. Wait, "Electromagnetic Radiation from Cylindrical Structures," New York: Pergamon Press 1959.

[19] L. B. Felsen, and N. Marcuvitz, "Radiation and Scattering of Waves," Chapters 4 and 5, Prentice Hall, Inc., 1973.

APPENDIX I. ASYMPTOTIC EVALUATION OF THE INTEGRALS

In this appendix one of the integral expressions encountered in Section II is evaluated asymptotically. The procedure serves as a recipe, all the expressions given in Equations (3) through (7) can be evaluated in the same fashion.

Consider now the integral

$$I = \int_{-\infty}^{\infty} e^{-jh(z-z')} \sum_{n=-\infty}^{\infty} A(n,h)\, e^{-jn(\phi-\phi')}\, dh \tag{42}$$

where

$$A(n,h) = \frac{hn}{\beta^2 a} \frac{H_n^{(2)'}(\beta\rho)}{H_n^{(2)'}(\beta a)} \tag{43}$$

and

$$\beta^2 = k^2 - h^2 \,. \tag{44}$$

The first essential step is to apply a Watson transformation to express the series in the integral as a contour integral in the manner [18]

$$\sum_{n=-\infty}^{\infty} A(n,h) e^{-jn(\phi-\phi')} = \frac{1}{2j} \int_{C_1+C_2} A(\nu,h)\, \frac{e^{j\nu\pi}}{\sin \nu\pi}\, e^{-j\nu|\phi-\phi'|}\, d\nu \tag{45}$$

where ν is a complex variable, and C_1+C_2 is a contour which encloses the poles of the integrand (i.e., the zeros of sin $\nu\pi$) as shown in Figure 12. Now the integral can be expressed as

$$I = \frac{1}{2j} \int_{-\infty}^{\infty} e^{-jh(z-z')} \int_{C_1+C_2} A(\nu,h)\, \frac{e^{j\nu\pi}}{\sin \nu\pi}\, e^{-j\nu|\phi-\phi'|}\, d\nu\, dh \tag{46}$$

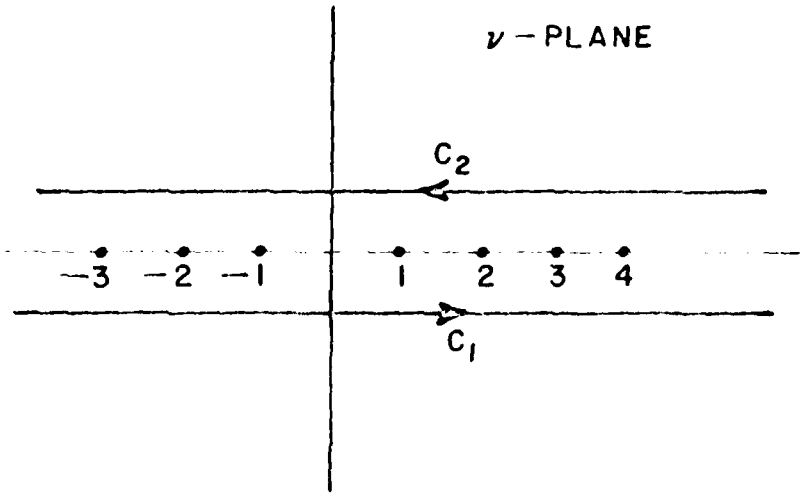

Figure 12. The integration contour in the complex ν-plane.

Replacing ν by -ν in the integral over C_2, it is seen that

$$\int_{C_2} A(\nu,h)\ \frac{e^{j\nu\pi}}{\sin \nu\pi}\ e^{-j\nu|\phi-\phi'|}\, d\nu = \int_{C_1} [-A(\nu,h)]\ \frac{e^{-j\nu\pi} e^{j\nu|\phi-\phi'|}}{\sin \nu\pi}\, d\nu \tag{47}$$

Substituting Equation (47) into Equation (46), one obtains

$$I = \frac{1}{2j} \int_{-\infty}^{\infty} e^{-jh(z-z')} \int_{C_1} \frac{e^{j\nu\pi}}{\sin \nu\pi}\ A(\nu,h) \left\{ e^{-j\nu|\phi-\phi'|} - e^{-j\nu[2\pi-|\phi-\phi'|]} \right\} d\nu\, dh \tag{48}$$

In this contour, $\mathrm{Im}(\nu) > 0$ and therefore it is permissible to write

$$\frac{e^{j\nu\pi}}{\sin \nu\pi} = 2j \sum_{m=0}^{\infty} e^{-j\nu 2\pi m} \tag{49}$$

which leads to

$$\epsilon = \sum_{m=0}^{\infty} [T_m(\alpha) - T_m(2\pi-\alpha)] \tag{50}$$

where

$$T_m(\alpha) = \int_{-\infty}^{\infty} e^{-jh(z-z')} \int_{C_1} A(\nu,h)\, e^{-j\nu(\alpha+2\pi m)}\, d\nu\, dh \tag{51}$$

in which $\alpha = |\phi-\phi'|$.

Substituting Equation (43) into (51) and keeping only the m=0 term, one obtains

$$T_0(\alpha) = \int_{-\infty}^{\infty} e^{-jh(z-z')} \int_{C_1} \frac{h\nu}{\beta^2 a} \frac{H_\nu^{(2)'}(\beta\rho)}{H_\nu^{(2)'}(\beta a)}\, e^{-j\nu\alpha}\, d\nu\, dh \tag{52}$$

Following a standard procedure (e.g., Reference [18]), one transforms variables via the relation

$$\nu = \beta a + \left(\frac{\beta a}{2}\right)^{1/3} t. \tag{53}$$

It follows from Wait [18] that in the shadow region, particularly in the case where $|\nu|$ and βa are both large and of the same order of magnitude, the Airy function approximation for the Hankel function $H_\nu^{(2)'}(\beta a)$ is given by

$$H_\nu^{(2)'}(\beta a) \approx \frac{-j}{\sqrt{\pi}} \left(\frac{2}{\beta a}\right)^{2/3} w_1'(t) \left\{1 + 0\left[t\left(\frac{2}{\beta a}\right)^{2/3}\right] \cdots\right\} \tag{54}$$

where $w_1'(t)$ is the Airy Integral [18] defined by

$$w_1'(t) = \frac{1}{\sqrt{\pi}} \int_{\Gamma_1} x\, e^{(tx-t^3/3)}\, dx \tag{55}$$

The contour Γ_1 is shown in Figure 13.

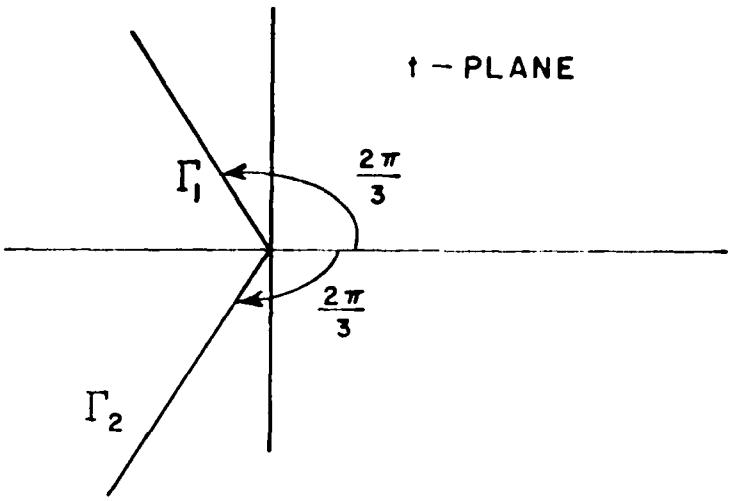

Figure 13. The integration contour in the complex t-plane.

Returning to Equation (52), one notes that $\beta\rho$ are greater than $\beta a \gtrsim \nu$; therefore, $H_{\nu(\beta\rho)}^{(2)'}$ may be replaced by their Debye asympotic form

$$H_\nu^{(2)'}(\beta\rho) \approx (-j)\sqrt{\frac{2}{\pi\beta\rho \sin\alpha_o}} \sin\alpha_o \, e^{-j\beta\rho(\sin\alpha_o - \alpha_o\cos\alpha_o)} e^{j\frac{\pi}{4}} \tag{56}$$

in which $\beta\rho\cos\alpha_o = \nu$ so that $\beta\rho\sin\alpha_o = (\beta^2\rho^2 - \nu^2)^{1/2}$. Now since $\nu \gtrsim \beta a$, it follows that $\beta\rho\sin\alpha_o \approx \beta(\rho^2 - a^2)^{1/2}$ and $\alpha_o \gtrsim \cos^{-1}(a/\rho)$. Therefore

$$H_\nu^{(2)'}(\beta\rho) \approx -j\sqrt{\frac{2j}{\pi\beta d}} \sin\alpha_o \, e^{-j\beta d} e^{j\nu\alpha_o} \tag{57}$$

where $d=(\rho^2-a^2)^{1/2}$ and α_0 are shown in Figure 14. Substituting Equations (54) and (57) into Equation (52), the function $T_0(\alpha)$ can now be written as

$$T_0(\alpha) = \int_{-\infty}^{\infty} e^{-jh(z-z')} \frac{h}{\beta^2 a} \int_{C_1} \left[\beta a + \left(\frac{\beta a}{2}\right)^{1/3} t\right] \tag{58}$$

$$\left[J\left(\frac{\beta a}{2}\right)^{2/3} \frac{1}{w_1'(t)}\right] \left[(-j)\sqrt{\frac{2j}{\pi\beta d}} \sin\alpha_0 \, e^{-j\beta d} \, e^{j\beta\alpha_0}\right]$$

$$e^{-j\beta\alpha} \, d\nu \, dh.$$

Making use of Equation (53), one transforms the integration from ν plane into t-plane and Equation (58) is now expressed as

$$T_0(\alpha) = \sin\alpha_0 \int_{-\infty}^{\infty} \left\{\frac{\pi h}{2\beta}\right\} \left\{\beta a \, g(\xi) + j\left(\frac{\beta a}{2}\right)^{1/3} g'(\xi)\right\} \tag{59}$$

$$\cdot \sqrt{\frac{2j}{\pi\beta d}} \; e^{-j\{h(z-z')+\beta[d+a(\alpha-\alpha_0)]\}} \, dh$$

where

$$\xi = \left(\frac{\beta a}{2}\right)^{1/3} (\alpha-\alpha_0) \tag{60}$$

and

$$g(\xi) = \frac{1}{\sqrt{\pi}} \int_{\Gamma_2} \frac{e^{-j\xi t}}{w_1'(t)} \, dt \tag{61}$$

$$g'(\xi) = \frac{-j}{\sqrt{\pi}} \int_{\Gamma_2} \frac{t \, e^{-j\xi t}}{w_1'(t)} \tag{62}$$

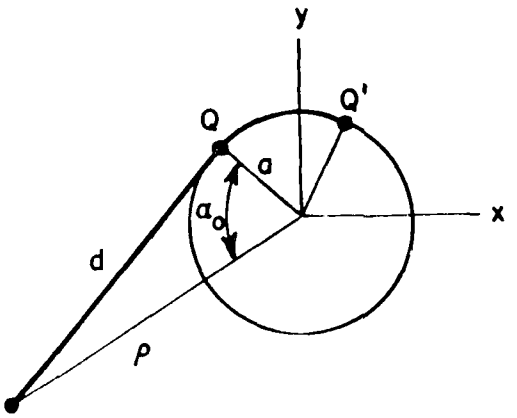

Figure 14. Ray geometry in the x-y plane.

Defining D sin δ = z-z' and D cos δ = d + a(α-α_o) and transforming the above integral $T_o(\alpha)$ into w-plane via $h = k \sin w$ [19], one obtains

$$T_o(\alpha) \approx \sin \alpha_o \int_{\bar{P}} \frac{\pi \sin w}{2 \cos w} \left\{ ka \cos w \, g(\xi) + j \left(\frac{ka \cos w}{2} \right)^{1/3} g'(\xi) \right\} \sqrt{\frac{2j}{\pi kd \cos w}} \; e^{-jkD \cos(w-\delta)} \; k \cos w \, dw \qquad (63)$$

where $\bar{P}$ is the integration path in the complex w-plane shown in Figure 15.

Equation (63) can be written in a form suitable for an asymptotic evaluation via the method of steepest descent:

$$T_o(\alpha) \approx \sin \alpha_o \int_{\bar{P}} f(w) \, e^{kD \, q(w)} \, dw \; . \qquad (64)$$

in which

$$f(w) = \frac{\pi}{2} \sin w \left\{ ka \cos w\, g(\xi) + j \left(\frac{ka \cos w}{2} \right)^{1/3} g'(\xi) \right\} k \cos w \int^{\infty} e^{-kd \cos} \quad (65)$$

and

$$q(w) = -j \cos (w-\delta) \quad (66)$$

where kD is the large parameter.

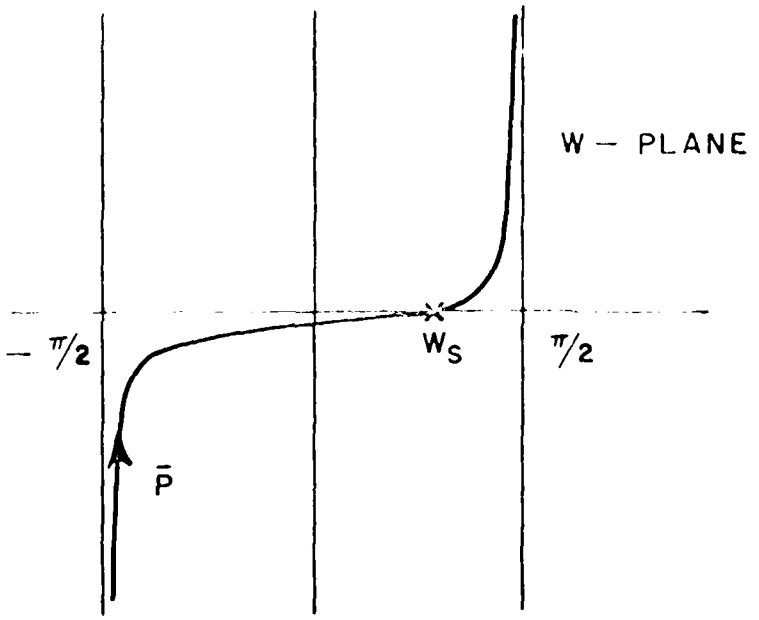

Figure 15. The integration path in the complex w-plane.

Using $q'(w_s) = 0$, the saddle point of the function q(w) can be found to be

$$w_s = \delta = \tan^{-1}\left(\frac{z-z'}{d + a(\alpha-\alpha_0)} \right) . \quad (67)$$

Let us now study the geometrical meaning of w_s. Figure 16 illustrates the geometry of the ray path from the source Q' to the field point P. It is evident from the developed view of Figure 16(c), that the path Q'QP minimized the distance between the source Q' and the field point P. A part of the ray path Q'Q lies on the cylinder surface, where it is a geodesic helix with pitch angle w_s. The tangent line QP, then, completes the ray path. Note that (see Figure 16)

$$\ell \cos w_s = a(\alpha-\alpha_o) \tag{68}$$

$$s \cos w_s = d \ . \tag{69}$$

and

$$D = s + \ell \tag{70}$$

From the standard procedure (e.g., see [19], the asymptotic approximation of the integral $T_o(\alpha)$ can be expressed as

$$T_o(\alpha) \sim \sqrt{\frac{2\pi}{kD\left|q''(w_s)\right|}} \ f(w_s) e^{kD\, q(w_s)} \ e^{j\frac{\pi}{4}} \tag{71}$$

where

$$q(w_s) = -j \tag{72}$$

and

$$q''(w_s) = j \tag{73}$$

and

$$f(w_s) = \left[\frac{\pi}{2} k^2 a \sin w_s \ g(\xi_s)\right. \tag{74}$$

$$\left. + j\frac{k}{2}\left(\frac{\sin w_s}{\cos w_s}\right)\left(\frac{ka \cos w_s}{2}\right)^{1/3} g'(\xi_s)\right] \frac{e^{-jk\ell}}{\sqrt{s}} \ e^{-jks} \ e^{j\frac{\pi}{4}}$$

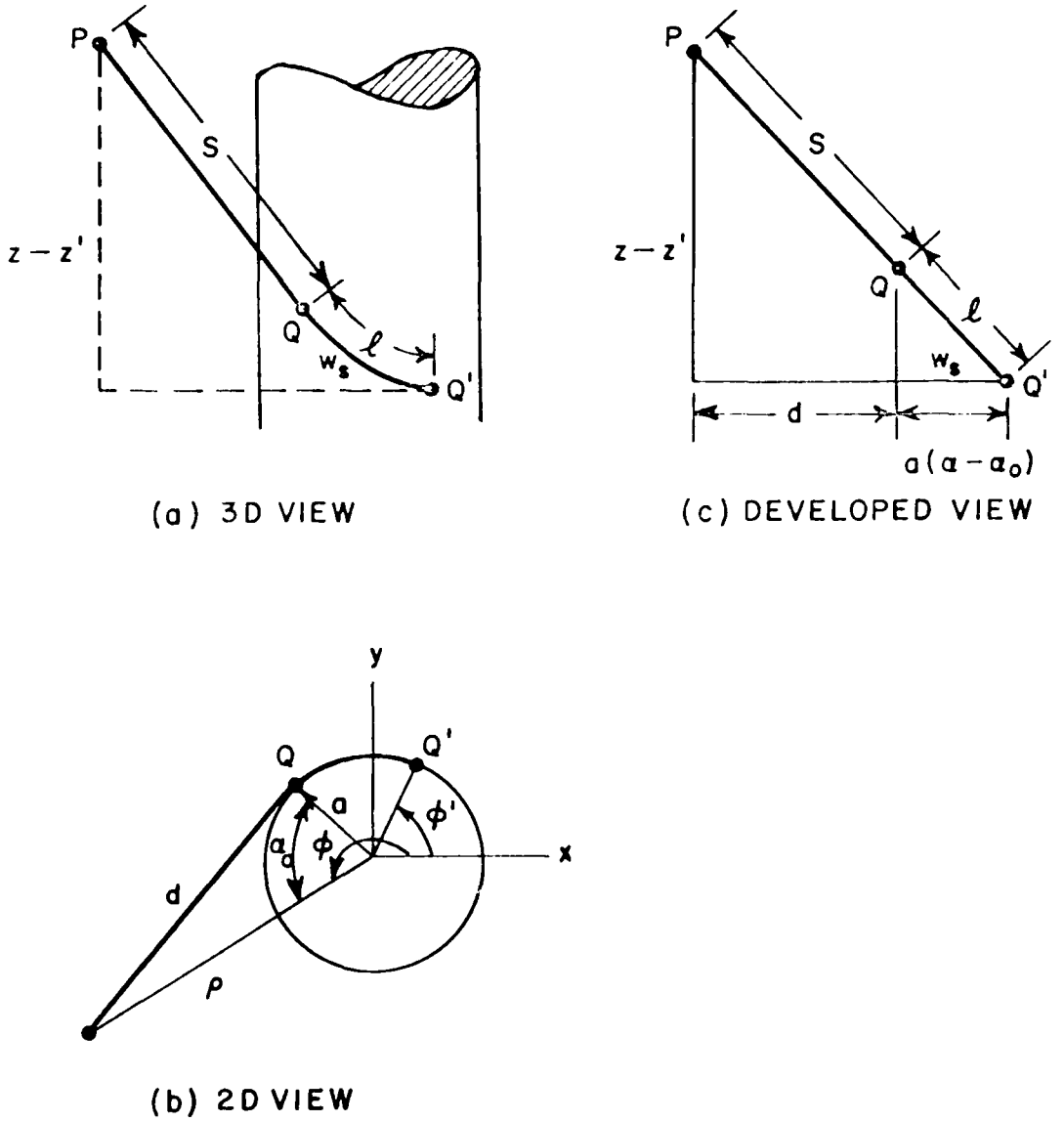

Figure 16. Geometry for the ray path.

Substituting Equations (72) through (74) into Equation (71), one finally obtains

$$T_0(\alpha) \sim \left[\frac{j}{2} k^2 a \sin w_s \, g(\xi_s) - \frac{k}{2} \left(\frac{\sin w_s}{\cos w_s} \right) \left(\frac{ka \cos w_s}{2} \right)^{1/3} g'(\xi_s) \right] \tag{75}$$

$$\frac{e^{-ik\ell} \, e^{-jks}}{\sqrt{s(s+\ell)}}$$

where

$$\xi_s = \left(\frac{ka \cos w_s}{2} \right)^{1/3} (\alpha - \alpha_0). \tag{76}$$

It should be noted that the second term in Equation (75) is a higher-order term. Usually it can be neglected. However, for some special situations, (e.g., see Figures 5 and 8 in Section IV) this higher-order term is important and should be included. For consistency, one then should also include the next higher order term for the Airy function approximation of Hankel function given by Equation (56).

APPENDIX II. LISTING OF THE COMPUTER PROGRAM GENERATING THE SOFT FOCK FUNCTION $g^S(x)$

$$g^S(x) = \begin{cases} G^*(x) = e^{+j\frac{x^3}{3}} \, g(x) & x \leq 0 \\ g^*(x) = g(x) & x \geq 0 \end{cases}$$

where $g(x)$ is the soft Fock function tabulated by Logan [9],

$$g(x) = \frac{1}{\sqrt{\pi}} \int_{-\infty}^{\infty} \frac{e^{ixt}}{w_1(t)} \, dt \, .$$

Note that Logan's table uses the time dependence e^{-jwt}.

```
      COMPLEX FUNCTION GB(X)
C****
C**** GB(X) IS RELATED TO THE FOCK FUNCTION (CURRENT DISTRIBUTION
C**** FUNCTION ) FOR THE SOFT CASE.
C**** FOR X<0.0  I.E. IN THE LIT REGION:
C****              GB(X)=CEXP(X**3/3.*J)*THE INTEGRAL OF
C****              CEXP(J*X*T)/W1(T)/SQRT(PI)
C**** FOR X>0.0  I.E. IN THE SHADOW REGION:
C****              GB(X)=THE INTEGRAL OF CEXP(J*X*T)/W1(T)/SQRT(PI)
C**** NOTE THAT THE TIME CONVENTION IS CEXP(-JWT)
C****
      DIMENSION XF(9),CL(9),VFL(9),VFD(9),PFL(9),PFD(9)
      DATA IN/0/
      DATA XF/.0,.5,1.,1.5,2.,2.5,3.,3.5,4./
      DATA VFD/.7758,.3829,.1673,.0665,.025,.0091,.0033,.00135,.0/
      DATA VFL/.7758,1.377,2.1605,3.063,4.024,5.010,6.004,7.002,8.001/
      DATA PFD/-60.,-35.07,.08,35.88,71.61,106.51,140.67,170.,200./
      DATA PFL/-60.,-75.54,-83.22,-86.78,-88.37,-89.12,-89.48,
     1-89.67,-89.78/
      PI=3.14159265
      SGN=SIGN(1.,X)
      IF(X.GT.4.) GO TO 2000
      IF(X.LT.-4.) GO TO 3000
      IF(IN.NE.0) GO TO 1
      DO 2 I=1,9
      CL(I)=1.
      DO 2 N=1,9
      DX=SGN*(XF(I)-XF(N))
      IF(ABS(DX).LT.1.E-6) DX=1.
      CL(I)=CL(I)*DX
2     CONTINUE
      IN=1
1     CONTINUE
      T=1.
      DO 3 N=1,9
      DX=X-XF(N)*SGN
      IF(ABS(DX).LT.1.E-6) GO TO 1000
      T=T*DX
3     CONTINUE
      VGB=0.0
      PGB=0.0
      DO 4 N=1,9
      VF=VFD(N)
      PF=PFD(N)
      IF(X.LT.0.0) VF=VFL(N)
      IF(X.LT.0.0) PF=PFL(N)
      C=CL(N)*(X-XF(N)*SGN)
      C=1./C
      VGB=VGB+C*VF
      PGB=PGB+C*PF
```

```
      4     CONTINUE
            VGB=VGB*1
            PGB=PGB*1
            GB=VGB*CEXP(CMPLX(.0,PGB*PI/180.))
            RETURN
 1000       VGB=VEL(I)
            PGB=PEL(I)
            IF(X.LT.0.0) VGB=VEL(I)
            IF(X.LT.0.0) PGB=PEL(I)
            GB=VGB*CEXP(CMPLX(.0,PGB*PI/180.))
            RETURN
 2000       GB=(.0,.0)
            RETURN
 3000       GB=(.0,1.)**(2.-(.0,1.)/(2.**3))
            RETURN
            END
```

x	$g^S(x)$ mag	phase (deg.)
-10.000	20.000	-89.986
-9.500	19.000	-89.983
-9.000	18.000	-89.980
-8.500	17.000	-89.977
-8.000	16.000	-89.972
-7.500	15.000	-89.966
-7.000	14.000	-89.958
-6.500	13.000	-89.948
-6.000	12.000	-89.934
-5.500	11.000	-89.914
-5.000	10.000	-89.885
-4.500	9.000	-89.843
-4.000	8.001	-89.780
-3.500	7.002	-89.670
-3.000	6.004	-89.480
-2.500	5.010	-89.120
-2.000	4.024	-88.370
-1.500	3.063	-86.780
-1.000	2.161	-83.220
-.500	1.377	-75.540
0.000	.776	-60.000
.500	.383	-33.370
1.000	.167	.000
1.500	.066	35.680
2.000	.025	71.610
2.500	.009	106.510
3.000	.003	140.670
3.500	.001	170.000
4.000	0.000	0.000
4.500	0.000	0.000
5.000	0.000	0.000
5.500	0.000	0.000
6.000	0.000	0.000
6.500	0.000	0.000
7.000	0.000	0.000
7.500	0.000	0.000
8.000	0.000	0.000
8.500	0.000	0.000
9.000	0.000	0.000
9.500	0.000	0.000
10.000	0.000	0.000

APPENDIX III. LISTING OF THE COMPUTER PROGRAM GENERATING THE HARD FOCK FUNCTION $g^h(x)$ and $\frac{d}{dx}[g^h(x)]$

$$g^h(x) = \begin{cases} G^*(x) = e^{j\frac{x^3}{3}} g(x) & x \leq 0 \\ G^*(x) = g(x) & x \geq 0 \end{cases}$$

where $g(x)$ is the hard Fock function tabulated by Logan [9].

$$g(x) = \frac{1}{\sqrt{\pi}} \int_{-\infty}^{\infty} \frac{e^{ixt}}{w_1(t)} \, dt \, .$$

Note that Logan's table uses the time dependence e^{-jwt}.

```
      COMPLEX FUNCTION G(X)
C****
C**** G(X) IS RELATED TO THE FOCK FUNCTION (CURRENT DISTRIBUTION
C**** FUNCTION ) FOR THE HARD CASE.
C**** FOR X<0.0  I.E. IN THE LIT REGION:
C****            G(X)=CEXP(X**3/3.*J)*THE INTEGRAL OF
C****            CEXP(J*X*T)/W1'(T)/SQRT(PI)
C**** FOR X>0.0  I.E. IN THE SHADOW REGION:
C****            G(X)=THE INTEGRAL OF CEXP(J*X*T)/W1'(T)/SQRT(PI)
C**** NOTE THAT THE TIME CONVENTION IS CEXP(-JWT)
C****
      DIMENSION XF(10),CL(10),VFL(10),VFD(10),PFL(10),PFD(10)
      DATA IN/0/
      DATA XF/.0,.25,.5,1.,1.5,2.,2.5,3.,3.5,4.55/
      DATA VFD/1.3994,1.232,1.0591,.7382,.4881,.3153,.2025,.13,
     1.0836,.0537/
      DATA PFD/.0,4.886,11.36,26.64,42.56,57.98,72.90,87.57,
     1102.17,116.75/
      DATA VFL/1.3994,1.552,1.662,1.961,1.948,1.982,1.994,1.998,
     1.9990,1.9995/
      DATA PFL/.0,-2.864,-3.9,-3.67,-2.42,-1.45,-.085,-.52,-.33,-.22/
      PI=3.14159265
      SGN=SIGN(1.,X)
      IF(X.GT.4.) GO TO 2000
      IF(X.LT.-2.5) GO TO 3000
      IF(IN.NE.0) GO TO 1
      DO 2 I=1,10
      CL(I)=1.
      DO 2 N=1,10
      DX=1.0*(XF(I)-XF(N))
      IF(ABS(DX).LT.1.E-6) DX=1.
      CL(I)=CL(I)*DX
2     CONTINUE
      IN=1
1     CONTINUE
      T=1.
      DO 3 N=1,10
      DX=X-XF(N)*SGN
      IF(ABS(DX).LT.1.E-6) GO TO 1000
      T=T*DX
3     CONTINUE
      VG=0.0
      PG=0.0
      DO 4 N=1,10
      VF=VFD(N)
      PF=PFD(N)
      IF(X.LT.0.0) VF=VFL(N)
      IF(X.LT.0.0) PF=PFL(N)
      C=CL(N)*(X-XF(N)*SGN)
      C=SGN/C
```

```
      VG=VG+C*VF
      PG=PG+C*PF
4     CONTINUE
      VG=VG*T
      PG=PG*T
      G=VG*CEXP(CMPLX(0.0,PG*PI/180.))
      RETURN
1000  VG=VFD(N)
      PG=PFD(N)
      IF(X.LT.0.0) VG=VFL(N)
      IF(X.LT.0.0) PG=PFL(N)
      G=VG*CEXP(CMPLX(0.0,PG*PI/180.))
      RETURN
2000  G=1.8325*CEXP(CMPLX(.0..5094*X))*EXP(-.2823*X)
      RETURN
3000  G=2.+(.0+1.)/(2.*)**3)-2./)**6
      G=G-(.0+2.)*7.326/X**9
      RETURN
      END
```

```
      COMPLEX FUNCTION GP(X)
C****
C**** GP(X) IS RELATED TO THE FOCK FUNCTION (CURRENT DISTRIBUTION
C**** FUNCTION ) FOR THE HARD CASE.(!!! THE DERIVATIVE OF G(X) !!!)
C**** FOR X<3.4  I.E. IN THE LIT REGION:
C****              GP(X)=CEXP(X**3/3.*J)*THE INTEGPRAL OF
C****              (J*T)*CEXP(J*X*T)/W1*(T)/SQRT(PI)
C**** FOR X>3.4  I.E. IN THE SHADOW REGION:
C****              GP(X)=THE INTEGPRAL OF (J*T)*CEXP(J*X*T)/W1*(T)/SQRT(PI)
C**** NOTE THAT THE TIME CONVENTION IS CEXP(-JWT)
C****
      COMPLEX G
      DIMENSION XF(10),CL(10),VFD(10),PFD(10)
      DATA IN/0/
      DATA XF/3.5,4.,4.5,5.,5.5,6.,6.5,7.,7.5,8./
      DATA VFD/.03520,.03476,.03522,.02266,.01458,
     1.00938,.00695,.00383,.00250,.00161/
      DATA PFD/252.21,256.78,281.35,295.93,310.52,
     1325.12,339.71,354.30,368.90,383.49/
      PI=3.14159265
      IF(X.GE.3.4) GO TO 1000
      IF(X.LT.-2.6) GO TO 3000
      XP=X+.001
      XM=X-.001
      GP=(G(XP)-G(XM))/(XP-XM)
      RETURN
 3000 CONTINUE
      SGN=SIGN(1.,X)
      IF(X.GT.0.) GO TO 2000
      IF(IN.NE.0) GO TO 1
      DO 2 I=1,10
      CL(I)=1.
      DO 2 N=1,10
      DX=1.0*(XF(I)-XF(N))
      IF(ABS(DX).LT.1.E-6) DX=1.
      CL(I)=CL(I)*DX
    2 CONTINUE
      IN=1
    1 CONTINUE
      T=1.
      DO 3 J=1,10
```

```
      DX=X-XF(I)*SGN
      IF(ABS(DX).LT.1.E-6) GO TO 4000
      T=T*DX
    3 CONTINUE
      VG=0.0
      PG=0.0
      DO 4 [illegible]
      F=[illegible]
      PF=PFD(M)
      C=CD(M)*(X-XF(M)*SGN)
      C=SGN/C
      VG=VG+C*VF
      PG=PG+C*PF
    4 CONTINUE
      VG=VG*T
      PG=PG*T
      GP=VG*CEXP(CMPLX(0.0,PG*PI/180.))
      RETURN
 4000 CONTINUE
      VG=VFD(M)
      PG=PFD(M)
      GP=VG*CEXP(CMPLX(0.0,PG*PI/180.))
      RETURN
 2000 GP=(0.0,0.0)
      RETURN
 3000 GP=(0.0,-1.5)/X**4+12./X**7
      RETURN
      END
```

	$g^h(x)$		$\frac{d}{dx}[g^h(x)]$	
x	mag	phase	mag	phase
-10.000	2.001	-.014	.000	-90.458
-9.500	2.001	-.017	.000	-90.535
-9.000	2.001	-.020	.000	-90.629
-8.500	2.000	-.023	.000	-90.746
-8.000	2.001	-.028	.000	-90.895
-7.500	2.000	-.034	.000	-91.086
-7.000	2.000	-.042	.001	-91.336
-6.500	2.000	-.052	.001	-91.669
-6.000	2.000	-.066	.001	-92.121
-5.500	2.000	-.086	.002	-92.753
-5.000	2.000	-.114	.002	-93.662
-4.500	2.000	-.157	.004	-95.017
-4.000	2.000	-.222	.006	-97.125
-3.500	1.999	-.329	.010	-100.569
-3.000	1.997	-.510	.019	-106.504
-2.500	1.994	-.850	.037	-112.528
-2.000	1.982	-1.450	.064	-128.783
-1.500	1.948	-2.420	.136	-144.958
-1.000	1.861	-3.670	.283	-168.666
-.500	1.682	-3.900	.471	168.969
0.000	1.399	0.000	.758	148.013
.500	1.059	11.360	.862	154.204
1.000	.758	26.640	.710	171.317
1.500	.488	42.560	.498	-170.019
2.000	.315	57.900	.324	-152.908
2.500	.202	72.900	.208	-137.257
3.000	.130	87.570	.133	-122.442
3.500	.084	102.170	.085	-107.790
4.000	.053	115.617	.055	-93.220
4.500	.035	131.339	.035	-78.650
5.000	.022	145.932	.023	-64.070
5.500	.014	160.526	.015	-49.480
6.000	.009	175.119	.009	-34.880
6.500	.006	-170.288	.006	-20.290
7.000	.004	-155.695	.004	-5.700
7.500	.002	-141.101	.002	8.900
8.000	.002	-126.508	.002	23.490
8.500	.001	-111.915	0.000	0.000
9.000	.001	-97.322	0.000	0.000
9.500	.000	-82.729	0.000	0.000
10.000	.000	-68.135	0.000	0.000

ACKNOWLEDGMENTS

Helpful discussions with Dr. P. Pathak and Dr. W. D. Burnside are truly appreciated.


DATE
ILME